



Article

$^{40}\text{Ar}/^{39}\text{Ar}$ Geochronology and New Mineralogical and Geochemical Data from Lamprophyres of Chompolo Field (South Yakutia, Russia)

Evgeny I. Nikolenko ^{1,2,*} , Konstantin V. Lobov ², Alexey M. Agashev ²,
Nikolay S. Tychkov ², Maria V. Chervyakovskaya ³, Igor S. Sharygin ⁴ and Anna M. Nikolenko ² 

¹ Geo-Scientific Research Enterprise ALROSA (PJSC), Chernyshevskoe Highway 16, 678170 Mirny, Republic of Sakha (Yakutia), Russia

² Sobolev Institute of Geology and Mineralogy, Siberian Branch of the Russian Academy of Sciences, pr. Akademika Koptiyuga 3, 630090 Novosibirsk, Russia; kost_1j@mail.ru (K.V.L.); agashev@igm.nsc.ru (A.M.A.); tykh@igm.nsc.ru (N.S.T.); nikolenkoam@igm.nsc.ru (A.M.N.)

³ Zavaritsky Institute of Geology and Geochemistry, Ural Branch of the Russian Academy of Science, Akademika Vonsovskogo Str. 15, 620016 Ekaterinburg, Russia; zaitseva.mv1991@gmail.com

⁴ Institute of the Earth's Crust, Siberian Branch of the Russian Academy of Sciences, Lermontov Str. 128, 664033 Irkutsk, Russia; isharygin@crust.irk.ru

* Correspondence: nevgeny@gmail.com

Received: 26 July 2020; Accepted: 30 September 2020; Published: 6 October 2020



Abstract: The alkaline igneous rocks of the Chompolo field (Aldan shield, Siberian craton), previously defined as kimberlites or lamproites, are more correctly classified as low-Ti lamprophyres. The emplacement age of the Ogonek pipe (137.8 ± 1.2 Ma) and the Aldanskaya dike (157.0 ± 1.6 Ma) was obtained using $^{40}\text{Ar}/^{39}\text{Ar}$ K-richterite dating. The Chompolo rocks contain abundant xenocrysts of mantle minerals (chromium-rich pyrope garnets, Cr-diopsides, spinels, etc.). The composition of the mantle xenocrysts indicates the predominance of spinel and garnet–spinel lherzolites, while the presence of garnet lherzolites, dunites, harzburgites, and eclogites is minor. The Chompolo rocks are characterized by large-ion lithophile element (LILE) and Light Rare Earth Element (LREE) enrichments, and high field strength element (HFSE) depletions. The rocks of the Ogonek pipe have radiogenic Sr ($^{87}\text{Sr}/^{86}\text{Sr}$ (t) = 0.70775 and 0.70954), and highly unradiogenic $\epsilon\text{Nd}_{(t)}$ (−20.03 and −20.44) isotopic composition. The trace element and isotopic characteristics of the Chompolo rocks are indicative of the involvement of subducted materials in their ancient enriched lithospheric mantle source. The Chompolo rocks were formed at the stage when the Mesozoic igneous activity was triggered by global tectonic events. The Chompolo field of alkaline magmatism is one of the few available geological objects, which provides the opportunity to investigate the subcontinental lithospheric mantle beneath the south part of the Siberian craton.

Keywords: Siberian craton; Aldan shield; alkaline magmatism; mantle source; lamprophyre; trace elements; isotopic data

1. Introduction

Studying the mineralogy and geochemistry of intraplate alkaline magmatism is one of the best tools we have to understand the composition and evolution of the deep continental lithosphere. Alkaline igneous rocks are products of the mantle melting processes and often contain mantle xenoliths and xenocrysts. These rocks are known to host economically significant deposits of critical metals such as Nb, Ta, and rare earth elements (REE) [1,2]. During the past few decades, increased attention has been given to high-Mg alkaline volcanism after the discovery of non-kimberlite diamond deposits,

such as those in the lamproites of Western Australia [3–5] and in alkaline lamprophyres [6], including the 2.7-Ga diamond-bearing lamprophyres from Wawa Superior Province, Canada [7].

Usually, occurrences of K-alkaline magmatism, according to their tectonic position, are subdivided into orogenic or anorogenic types [8], and characterized by specific geochemical features (reflected in the concentration of Ti, Nb, Zr and other elements). These geochemical differences are conditioned by subduction-related (or collision) tectonic setting and suggest an important role of “crustal” material in their petrogenesis. In some cases, the “orogenic” geochemical signatures are observed in the alkaline rocks formed in the stable cratonic setting. Relevant characteristics provide evidence about the complex geological history of the region and suggest the formation of a mantle source of K-rich melts long before the melts’ emplacement [8,9]. The rocks of Aldan alkaline province of Mesozoic magmatism, which formed in the ancient cratonic setting, also belong to the aforementioned category and demonstrate that geochemical signatures of ancient subduction processes were involved in producing the ancient source of potassic magmatism [10,11].

There are numerous manifestations of alkaline magmatism in the Aldan province of the Siberian craton (Yakutia, Russia), which were intruded over a spectrum of ages in the early and late Proterozoic, Devonian, Mesozoic and Cenozoic times [12,13]. The two largest events formed the Early Proterozoic Chara–Aldan (1818–1870 Ma) and Mesozoic Lena Aldan sub-provinces [14,15], which include several alkaline rock fields: the Tobuk–Khatystyr field, the Lower and Upper Yakokut fields, and the Murun and Lomam plutons (Figure 1) [11,14,16–18].

The alkaline igneous rocks of Chompolo field were first discovered in 1957–1958; they were initially classified as kimberlites due to their typical mineralogy, including mantle-derived pyrope, Cr-spinel, and Cr-diopside [19]. The rocks were also categorized as kimberlites in later studies [20–24]. However, alternative interpretations of the Chompolo rocks categorized them as lamprophyres or lamproites [11,14,16,18,25,26]. The above-listed papers presented petrographic, mineralogical and chemical data mainly discussing the ‘Aldan lamproites’, including the well-investigated rocks of the Tobuk–Khatystyr field, the Lower and Upper Yakokut fields, and the Murun and Lomam plutons. Some authors attributed the Chompolo rocks to the Aldan lamproite series without evidence [11]. Kornilova [25] first indicated the difference between the Chompolo rocks and kimberlites or lamproites.

Lamprophyric rocks have been misclassified as kimberlites previously. For example, the lamprophyres of the Navajo field were initially also called kimberlites [27]. Such confusion is related to the similarity in the texture of the brecciated rocks, the presence of xenocrysts of high-pressure mantle minerals, and the attempt to discover potentially diamondiferous kimberlites. In this study, we present new geochronological, isotopic, geochemical and mineralogical data on the Chompolo rocks and insights into the mantle source of these rocks.

2. Geological Background

The Siberian craton ($\sim 4 \times 10^6$ km², also referred to as the North Asian craton) was assembled by the accretion of Archean cratons and Paleoproterozoic and Mesoproterozoic terranes. The main stage of the complicated process of craton formation was 3.4–3.1 Ga [28], followed by stages of metamorphism and tectonic amalgamation at periods of 2.5–2.7 and 2.0–1.9 Ga, respectively [29,30].

The Chompolo field of alkaline magmatism is located within the Amga tectonic mélange zone in the southern part of the Siberian craton (Figure 1). The Amga tectonic mélange zone was formed at 1.9 Ga [31] and separates the West Aldan granite–greenstone terrane and the Central Aldan granulite–orthogneiss superterrane (Figure 1). The Amga zone is represented by a series of sub-meridional faults, separating fragments of the Archean and Early Proterozoic granulite–orthogneiss and granite–greenstone complexes. In terms of kinematics, thrust faults and strike–slip faults prevail among the faults of the Amga zone. The West Aldan composite terrane (WAD) consists of several terranes represented by orthogneisses of tonalite–trondhjemitic composition and greenstone belts of Archean age. The WAD terrane accretion occurred about 2.6 Ga and was accompanied by granite formation (Charodakan Granite Complex) and granulite metamorphism of all complexes [30,31].

The Central Aldan Superterrane (CA), consisting of the Archean and Paleoproterozoic rocks of the Nimnyr granulite–orthogneiss and the Sutam granulite–paragneiss terranes (Figure 1), dates to the peak of metamorphism around 2.1–1.9 Ga [31].

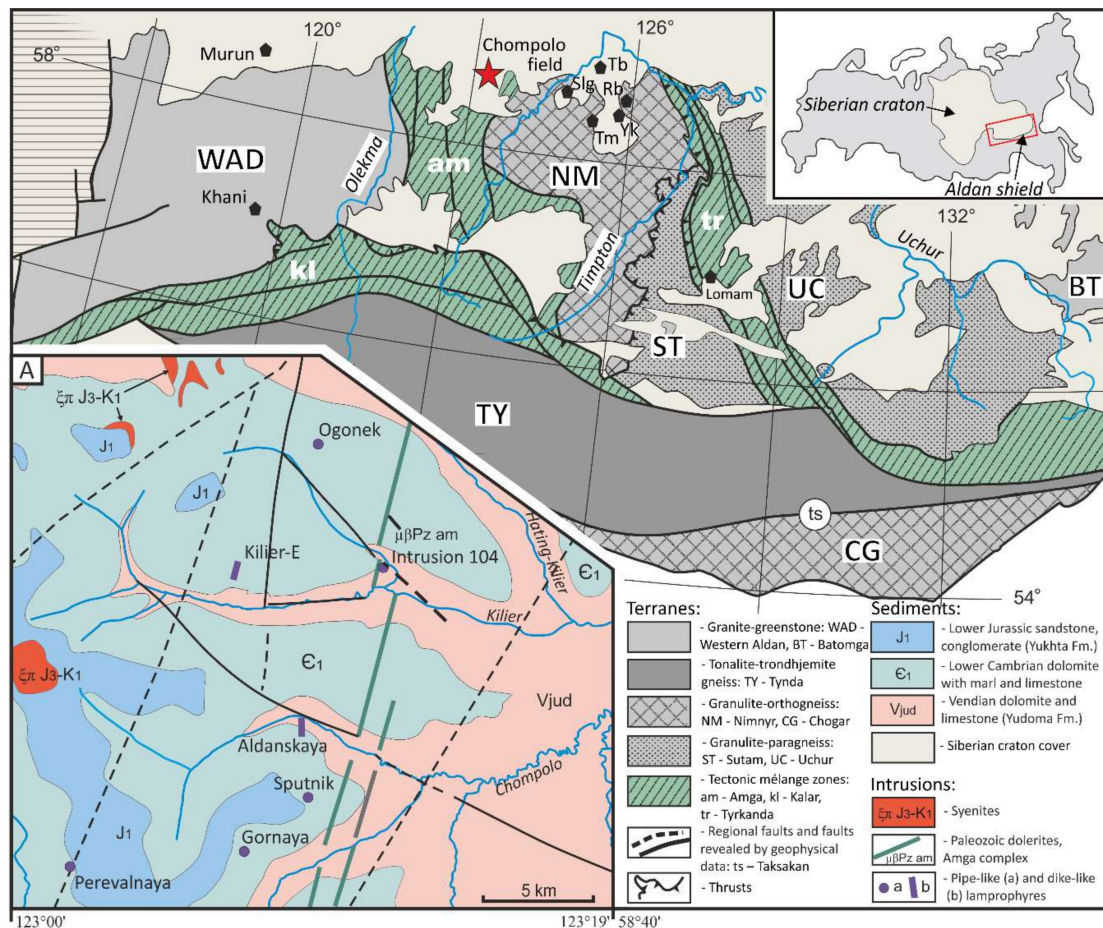


Figure 1. Tectonic structure of the Aldan–Stanovoy shield (modified from [30]) and local geology of the Chompolo field (A). Black pentagons mark the locations of alkaline rock fields and massifs: Rb—Ryabinoviy; Tm—Tommot; Sg—Seligdar; Tb—Tobuk–Khatystyr field, Yk—the Lower and Upper Yakokut fields.

The early Paleoproterozoic stage of the Siberian craton formation is reflected in multiple subduction, collision and accretion events that provide evidence for the merging of the terranes into the general present-day structure of the Siberian craton. Between 2.5–2.0 Ga, the Central Aldan, Daldyn and Tyung terranes formed a single amalgamated block accompanied by the Billyakh–Fedorov island arc and a concurrently subducting oceanic crust under the newly formed crustal block [32,33].

Within the Aldan province, multiple alkaline magmatic events occurred in the early and late Proterozoic, Devonian, Mesozoic and Cenozoic times [12,13]. The most voluminous Mesozoic magmatic activity includes several magmatic pulses and occurred during the range from 180 to 120 Ma, with temporal progression from subalkaline to potassic and ultrapotassic magmatism [11,34,35]. The Mesozoic stage was characterized by a wide diversity of alkaline rocks with ultramafic to silica-rich compositions, which form large massifs of complex composition, ring volcanic–plutonic complexes, dykes, diatremes, subvolcanic bodies, laccoliths. It is believed that the stage of Mesozoic igneous activity was triggered by the global tectonic events related to the final closure of the Mongol–Okhotsk Ocean south of the Aldan shield [10,36].

The geological structure of the Chompolo area involves the formation of two structural levels: a crystalline basement and a platform cover. The lower structural level is represented by Archean

quartzites and high-alumina gneisses. Sediments of the upper structural level belong to the Late Proterozoic–Early Cambrian age, and are represented by dolomites and limestones with interlayers of conglomerates and sandstones with carbonate cement (Figure 1). The Chompolo field is comprised of magmatic pipe-like bodies (e.g., the Ogonek, Gornaya, Sputnik, Pereval'naya, and Intrusions 29 and 104), some of which are complicated by apophyses, dyke bodies (e.g., Aldanskaya and Kilier-East) and veins (e.g., Osenniye) [37]. The thoroughly explored Aldanskaya dyke extends for 800 m with a width of 25 m. Ogonek is described as consisting of an isometric main body 80 m × 100 m and a dyke more than 250-m long in its northern part. The Chompolo lamprophyres are located in an area of about 25 km × 10 km (Figure 1A) and are confined to one local tectonic zone. There are four main fault directions within the Chompolo field, but alkaline rocks are related only to the sub-meridional fault system. Morphologically, the faults represent fractures with displacement amplitudes of 40–60 m at sub-vertical angles. This fault system, which is up to 45 km in length, is associated with different rock types of various ages, suggesting a long history of active movement [38].

Repeated attempts to determine the age of Chompolo rocks have not yet yielded reliable results. The available age estimates of the Chompolo rocks are controversial. A pre-Jurassic age has been suggested based on the discovery of pyropes in Lower Jurassic sediments [37], and a post-Early Triassic age was inferred by Bogatikov et al. [14], while Rb-Sr isochron dating of lamprophyre from Intrusion 104 (bulk sample) gave a younger age of 131 ± 4 Ma [39].

3. Sampling and Analytical Techniques

3.1. Sample Preparation

Only the near-surface zone of the investigated rock bodies was available for sampling. Rock and mineral samples were collected from seven bodies (Aldanskaya, Ogonek, Sputnik, Gornaya, Perevalnaya, Kilier-East and Intrusion 104) during fieldwork in 2012 and 2013 (Figure 1A, Table 1). The heavy mineral fractions were separated by gravity differentiation in the water and then by using bromoform with a specific gravity of 2.89.

Before conducting whole-rock analyses, the samples were pre-sawn into 3–5-mm-thick slabs from which central parts were selected for analysis. The selected fragments were crushed into 1–2-mm grains and cleaned of obvious xenogenic particles under a binocular microscope. The resulting pure samples were then triturated in an agate mortar.

Garnet, pyroxene, spinel, amphibole, mica, and apatite samples 0.5–3 mm in diameter were picked from heavy mineral fractions for detailed investigations. Sample preparation included mounting mineral grains in epoxy resin and cutting and grinding to reveal grain centers, followed by a final polish.

3.2. Analytical Methods

Investigations were carried out at the Analytical Center for Multi-Elemental and Isotope Research, Siberian Branch, at the Institute of Geology and Mineralogy, Siberian Branch of the Russian Academy of Sciences (IGM SB RAS, Novosibirsk).

The petrography of the rocks was examined in thin sections using a petrographic polarizing microscope (OLYMPUS BX-51, Olympus Corporation, Tokyo, Japan). Mineral chemistry was determined on a JEOL JXA-8100 electron microprobe (JEOL Ltd., Tokyo, Japan) with an accelerating voltage of 20 kV, a beam current of 50 nA [40], and a counting time of 5 s for background and 10 s for peaks. The same spot diameter of 2.5–3 μm was used for all minerals. The following standards were used for the quantification of the elements: diopside (Si-K α , Ca-K α), albite (Na-K α), fluorophlogopite (F-K α , K-K α), TiO₂ (Ti-K α), Fe₂O₃ (Fe-K α), NdPO₄ (Nd-L α), PrPO₄ (Pr-L α), CePO₄ (Ce-L β), LaPO₄ (La-L α), Sr-glass (Sr-L α), Ba-glass (Ba-L α). The analytical data were reduced using CITZAF procedures. Detection limits were <0.05 wt% for all elements analyzed. The energy-dispersive spectroscopy (EDS) analyses of minerals in thin sections were carried out on a Tescan MIRA 3 LMU scanning electron microscope (TESCAN, Brno, Czech Republic) coupled with an INCA EDS 450 microanalysis system

with a liquid nitrogen-free large-area EDS X-Max-80 Silicon Drift Detector (Oxford Instruments, Oxford, UK). The analytical conditions were 20 kV, 1 nA and a signal accumulation time of 40 s.

Whole-rock compositions were measured by X-ray fluorescence analysis (ARL-9900-XP spectrometer, Applied Research Laboratories, Austin, TX, USA). For the analysis, the sample powder was fused at a ratio of 1:9 with a mixture of lithium tetraborate, lithium metaborate, and lithium bromide to prepare glass beads. The detection limits were 0.05 wt% for MgO, 0.04 wt% for Na₂O, and 0.01 wt% for other major oxides. The loss on ignition (LOI) was measured by weight loss calculating after sample heating during 2.5 h at a temperature of 960 °C. Trace elements of the whole-rock samples were determined on a Finnigan MAT ELEMENT high-resolution inductively coupled plasma mass spectrometer with a U-5000AT+ ultrasonic nebulizer (Teledyne Cetac, Omaha, NE, USA). Samples were digested using the Li metaborate fusion method and subsequent dissolution of the fusion in dilute HNO₃. This method makes it possible to expand the list of analyzed elements (including Rb, Sr, Y, Ba, Th, and U) without changing the sample preparation conditions [41]. The calibration was carried out against the BHVO-1 external standard. For most of the elements, the standard deviation from the average was less than 5%.

The ⁴⁰Ar–³⁹Ar dating was performed on two grains of K-richterite by nine- and ten-step heating in the temperature range from 500 to 1130 °C [42]. K-richterite grains, together with biotite MSA-11 (age 311.0 ± 1.5 Ma) used as monitor, were placed into an Al-foil package and stacked in a silica tube. For the calibration of the weighted standard samples of biotite MSA-11, the international standard biotite (Lp-6) and muscovite (Bern 4 m) were used [43]. The silica tubes were irradiated in the water-cooled channel of the research reactor of Tomsk Polytechnic University (PTI TPU). The temperature in the reactor did not exceed 100 °C. The Ar isotope composition was measured on the ARGUS multi-collector mass spectrometer from GV-Instruments, Wythenshawe, Manchester, UK. Before the measurements, the samples were outgassed at 300 °C. Additional purification of Ar took place in Zr and Ti-Al SAES getters which were cooled by liquid nitrogen. The measurement errors given in the text and in the figures are ±1σ.

Confocal Raman spectroscopy study was performed on a Horiba Jobin Yvon LabRAM HR800 microspectrometer (HORIBA, Kyoto, Japan) with a 532.1 nm Ar laser equipped with an Olympus BX41 microscope (Olympus Corporation, Tokyo, Japan). We used the OPUS 5.0 software (Bruker Optik GmbH, Ettlingen, Germany) for the peak position fitting in the Raman spectra and the RRUFF project database and CrystalSleuth application (<http://rruff.info/>) for mineral identification [44].

Determinations of isotope composition and concentrations of Rb, Sr, Sm and Nd were conducted at the Institute of Geology and Geochemistry, Ekaterinburg, Russia. The weight of the dissolved samples was 100 mg, with isotope tracer added to each sample to determine the concentration of elements through the isotope dilution method. Chemical separation of Rb and Sr was performed using 2 mL of cation-exchange resin Bio-Rad AG 50 × 8, followed by purification of Sr in 3.7 mL of resin. Separation of Sm and Nd was performed in two stages following the method of Pin et al. [45], involving the collection of total REE using Bio-Rad AG 50 × 8 resin and subsequent separation of Sm and Nd by step eluting through LN7a resin. More detail information about isotopic analyses is provided in the Supplementary Materials.

Isotope compositions were analyzed in static mode on a TRITON Plus multicollector mass spectrometer (Thermo Fisher Scientific (Bremen) GmbH, Germany). The total procedural blank concentrations were 0.02, 0.2, 0.1 and 0.08 ng for Rb, Sr, Nd and Sm, respectively. The measured ⁸⁷Sr/⁸⁶Sr and ¹⁴³Nd/¹⁴⁴Nd ratios were normalized to ⁸⁸Sr/⁸⁶Sr = 8.37521 and ¹⁴⁸Nd/¹⁴⁴Nd = 0.24157. During this study, the analytical results for standards were as follows SRM 987 ⁸⁷Sr/⁸⁶Sr = 0.710256 (±11) and Nd IGM ¹⁴³Nd/¹⁴⁴Nd = 0.512402 ± 9, which corresponds to La Jolla ¹⁴³Nd/¹⁴⁴Nd = 0.511851. Multiple analyses of the BHVO-2 standard show the 0.2% precision of the ¹⁴⁷Sm/¹⁴⁴Nd ratio determinations. The calculation of εNd and Sm–Nd model age (TDM) used modern values for homogeneous chondrite reservoir (CHUR)—¹⁴³Nd/¹⁴⁴Nd = 0.512630, ¹⁴⁷Sm/¹⁴⁴Nd = 0.1960 [46], and depleted mantle (DM)—¹⁴³Nd/¹⁴⁴Nd = 0.513151, ¹⁴⁷Sm/¹⁴⁴Nd = 0.2136 [47].

4. Results

4.1. Petrography

Chompolo igneous rocks are dominantly inequigranular medium to fine clastic volcanic breccias with a flow texture and a medium- to fine-grained matrix (Figure 2a). The rocks show variable degrees of post-magmatic alteration. In contrast, Pereval'naya and Intrusion 104 pipe rocks have a massive structure and do not contain much country rock clastic material (5–10 vol%) (Figure 2g–i). These rocks have a porphyritic texture with 15–30% phenocryst content (Table 1). Rocks from the Aldanskaya, Sputnik, Gornaya, Ogonek and Kilier-East bodies have a variation in volcanoclastic texture. Autoliths and wall-rock clasts occupy 20% to 60% of the rock volume. Autoliths are less abundant and include numerous feldspar laths and variable amounts of opaque minerals (Figure 2b,c), and are similar to the breccia matrix in terms of their mineral composition. Quartzites (32%), gneiss (28%), leucogranites (24%), and granites (7%) were noted among the studied crustal xenoliths. A few garnet-bearing microxenoliths of the lower crust were also found. Sedimentary rocks and a variable amount of mica minerals were also present (Figure 2d).

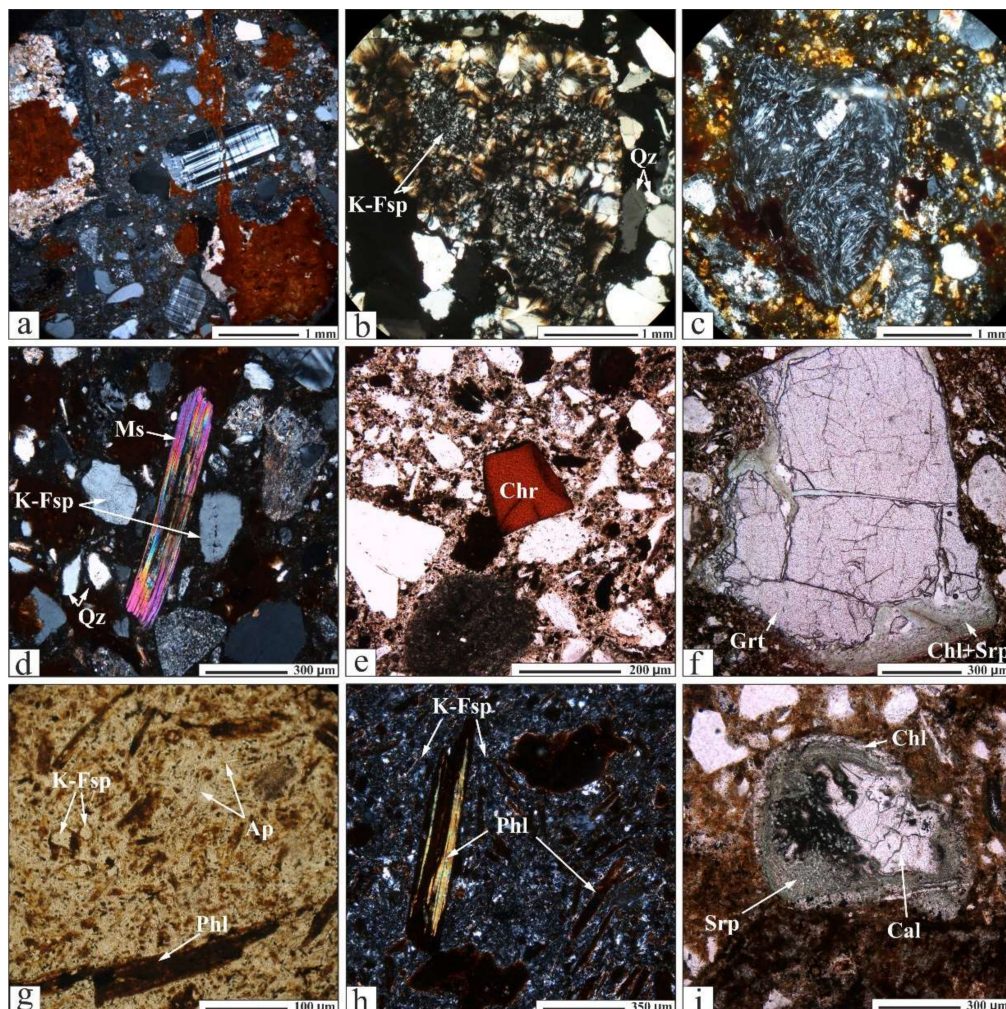


Figure 2. Photomicrographs of medium- to fine-clastic volcanic breccias and a fine-grained matrix Ogonek pipe (a,d); autoliths from Gornaya (b) and Perevalnaya (c) pipes; Cr-spinel (e) and garnet (f) xenocrysts from Ogonek volcanic breccias; Apatite accessory phase in the matrix of Intrusion 104 rocks' (g); K-feldspar (sanidine) in the cryptocrystalline matrix and phlogopite microphenocrysts replaced by secondary reddish-brownish aggregates of the Intrusion 104 rocks' (h); pseudomorphs after olivine in the Pereval'naya pipe rocks' (i). Abbreviations based on [48].

Table 1. The mineral assemblage of Chompolo rocks.

Name Lat./Long.	Cognate Minerals			Mantle Xenocrysts	Secondary Minerals
	Matrix	Phenocrysts	Accessory Minerals		
Aldanskaya 58°43'56.7"/123°09'22.4"	Kfs, Phl	Phl, Amp (Prg-Ed), Di-Aug, Ol ¹		Prp, Di, Ol ¹ , Cr-Spl, Pilm	Cal, Chl, Sme, Kln, Vrm
Ogonek 58°49'51.7"/123°09'54.8"	Kfs, Phl	Phl, rare Di-Aug, Ol ¹	Ap	Prp, Di, Ol ¹ , Cr-Spl	Cal, Chl, Gth, Sme, Kln, Vrm, Qz
Gornaya 58°41'20.5"/123°06'38.8"	Kfs, Phl	Di-Aug, Phl	Ap	Prp, Di, En, Ol ¹ , Cr-Spl,	Chl, Sme, Vrm, Gth
Sputnik 58°42'24.8"/123°09'38.5"	Kfs	Phl, Amp (Mg-Hbl), Ol ¹	Ap	Prp, Di, Ol ¹ , Cr-Spl,	Chl, Sme, Vrm, Gth,
Pereval'naya 58°40'51.9"/122°59'58.6"	Kfs, Phl	Di-Aug, Phl, rare Amp	Ap	Prp, Di, Cr-Spl,	Cal (Dol), Hem, Qz
Intrusion 104 58°47'18.4"/123°12'40.5"	Kfs, Phl	Di-Aug, Phl, Ol ¹ , rare Amp	Ap	-	Chl, Sme, Vrm

Abbreviations based on [48]: Cr-Spl—chromium spinel, Di-Aug—diopsidic augite, Mg-Hbl—magnesian hornblende, Prg-Ed—pargasite-edinite, Ol¹—pseudomorphs after olivine, Pilm—picroilmenite. Lat./Long.—Latitude/Longitude.

The modal mineralogy of the studied rocks is listed in Table 1. K-feldspar (sanidine), phlogopite, chlorite, and opaque minerals are the main minerals of the cryptocrystalline matrix (Figure 2). The variety of K-feldspar of magmatic origin appears as 20–100 µm prismatic microphenocrysts of sanidine. The interclast material of the Aldanskaya dyke and the Sputnik and Ogonek pipes also contain melanocratic phenocrysts, which are represented by alkali amphiboles or chloritized phlogopite with reddish-brownish aggregates, possibly formed by the replacement of the mica minerals (Figure 2h). Gornaya and Pereval'naya phenocrysts are clinopyroxene and phlogopite. Intrusion 104 phenocrysts are clinopyroxene, phlogopite and rare amphibole. Olivine in the Chompolo rocks is represented as pseudomorphs of serpentine, chlorite, carbonate aggregates, and found in the Pereval'naya, Ogonek, Sputnik, Intrusion 104 pipes and in the Aldanskaya dyke samples taken from 5 m below the surface. (Figure 2i). Altered olivine crystals are difficult to divide into xenocrystic and phenocrystic ones. Given the presence of mantle xenocrysts in the Chompolo rocks, olivine is represented by both varieties.

Apatite is an accessory phase and occurs in rocks as 10–50 µm euhedral grains (Figure 2g). All samples contain mica, vermiculite, smectite, kaolinite, and chlorite as replacement phases of feldspar or mica.

Opaque minerals are represented by magnetite and rare grains of rutile, as well as sulfides (pyrite, pentlandite). In most cases, the Fe-bearing opaque minerals in the rock matrix are replaced by secondary hydroxide minerals.

Xenocrysts include garnets, pyroxenes, amphiboles, Cr-spinel, as well as sporadic rutiles and zircons, and solitary grains of ilmenite (Figure 2e). Garnets vary in color from orange to saturated purple without any visual inhomogeneity and are characterized by an irregular or rounded shape.

They are usually coated with secondary mineral aggregates (chlorite and carbonate) (Figure 2f). Most of the Cr-spinel grains are rounded or sometimes perfectly shaped octahedra, but some have irregular shapes. The latter are common of interstitial spinels found in xenoliths of spinel and garnet-spinel peridotite, pyroxenite and in kimberlite-hosted garnet-spinel-pyroxene intergrowths [49]. Among clinopyroxenes, zoned grains with sharp-bordered outer rims are present (Figure S1). The Cpx rims often contain mineral inclusions represented by spinels, olivines, amphiboles or phlogopites.

No ilmenite was detected in thin sections by optical microscopy, and only trace amounts were found as small broken fragments (0.5–1 mm) in heavy mineral concentrate samples of eluvium from Chompolo rocks.

4.2. Geochronology

We used ⁴⁰Ar–³⁹Ar K-richterite dating to determine the age of the rocks from the Aldanskaya dyke and Ogonek pipe. Age determinations were carried out on two relatively large grains of K-richterite with weights of 24.79 mg (Ogonek) and 30.59 mg (Aldanskaya). These amphibole grains were

hand-picked from the heavy mineral concentrates and verified to be K-richterite by means of Raman spectroscopy. The high isotopic system closure temperature of the amphiboles (500–550 °C) [50,51] provided a minimal gap between the emplacement of the magmatic body and the starting of the ‘isotopic clock’. Seven temperature steps for each sample, accounting for 99% of the gas released, formed a finely defined plateau age of 157.0 ± 1.6 Ma and 137.8 ± 1.2 Ma for 13Al507 (Aldanskaya) and 13Al613 (Ogonek), respectively (Figures 3 and S2, Table S1).

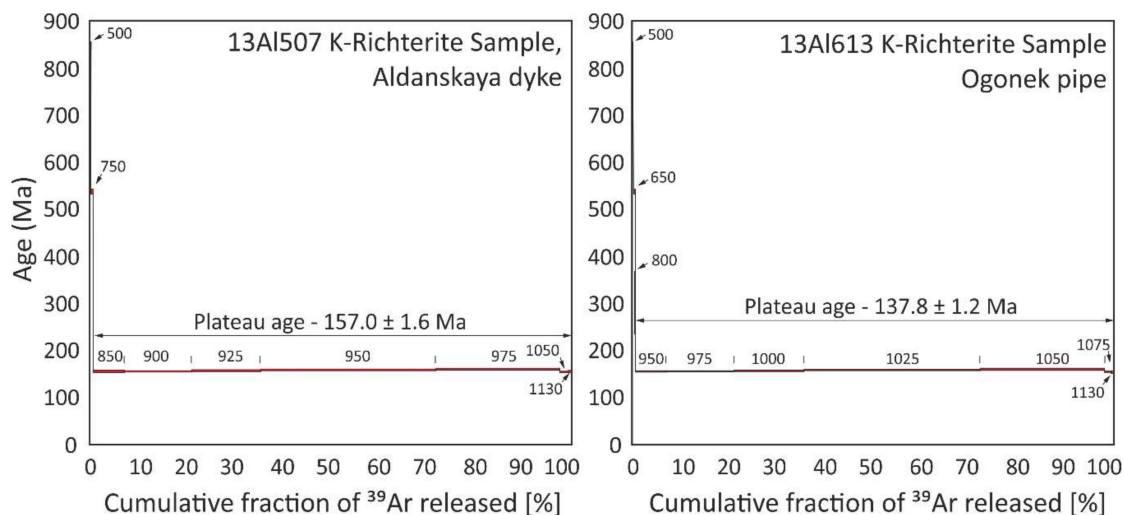


Figure 3. ^{40}Ar – ^{39}Ar plateau ages of K-Richterite (13Al507 and 13Al613) samples from Aldanskaya and Ogonek alkaline rocks of Chompolo field. The temperatures for each step of heating are shown (°C).

4.3. Mineral Chemistry

4.3.1. Olivine

Published data on the composition of olivines from the Chompolo rocks are restricted to $\text{Mg\#} = \text{Mg}/(\text{Mg} + \text{Fe}) = 0.94\text{--}0.95$ and CaO contents from 0.25–0.34 wt% [22].

Olivine inclusions were also found in the rims of zoned clinopyroxene grains (Figures 4 and S1). Olivine inclusions are characterized by relatively low $\text{Mg\#} = 0.81\text{--}0.87$ and concentrations of $\text{MnO} = 0.23\text{--}0.35$ wt%, $\text{CaO} = 0.21\text{--}0.48$ wt%, and $\text{NiO} = 0.27\text{--}0.33$ wt%.

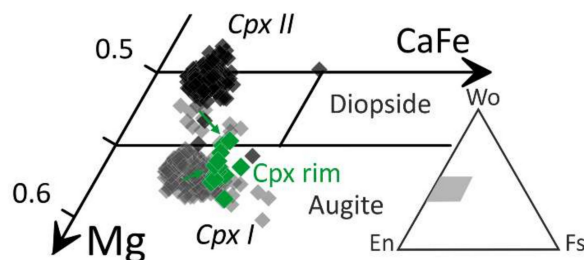


Figure 4. Pyroxene compositions projected onto the pyroxene classification diagram En-Fs-Wo [52]. Green rhombs represent the composition of the clinopyroxene rims; arrows reflect directions of chemical composition change from cores to rims.

4.3.2. K-Feldspar

The varieties of K-feldspar usually contains <1 wt% Na_2O (sometimes up to 3 wt% Na_2O) and 0.3–0.8 wt% Fe_2O_3 . Contents of BaO up to 1.8 wt% may occur in the outer part of the zoned sanidine grains. The fine-grained matrix of the breccias contains large quantities of sanidine that are characterized by Fe_2O_3 content in amounts of 0.3–1.5 wt%.

4.3.3. Clinopyroxene

Clinopyroxenes (Cpx) occur as isolated 0.2–2.0 mm grains in heavy mineral concentrate samples, some enclosing or intergrown with opaque minerals. All studied clinopyroxenes from Chompolo rocks are Mg-augites (Cpx I group) or diopsides (Cpx II group) according to the classification scheme in the system $\text{MgSiO}_3\text{--FeSiO}_3\text{--CaSiO}_3$ (Figure 4, Table S2) [52].

Mg-augites represent Cpx group I, which is characterized by low $\text{Mg}/(\text{Mg} + \text{Fe}_{\text{tot}})$ and $\text{Ca}/(\text{Ca} + \text{Mg} + \text{Fe}_{\text{tot}})$ molar ratios ($\text{Mg}\# = 0.85\text{--}0.94$; $\text{Ca}_{\text{ko}} = 0.41\text{--}0.48$, respectively). Mg-augites prevail in the Perevalnaya pipe (87% of all clinopyroxenes) and occur in lesser amounts in the Gornaya pipe and Aldansky dyke (36% and 22%, respectively). The rocks of the Ogonek pipe contain only about 1% of the group I Cpx, and they are totally absent in the Sputnik pipe. This group of pyroxenes is characterized by a significant difference in chemical composition relative to other Cr-diopsides and can be easily distinguished by its low Al_2O_3 (0.17–0.86 wt%) and Cr_2O_3 (0.21–1.42 wt%) content. In addition to the low number of trivalent cations, the group I clinopyroxenes are characterized by low Na_2O contents in the range of 0.43–0.99 wt% (average 0.58 wt%). The amount of FeO is in the range of 2.1–5.6 wt% (on average 3.32 wt%) and the MnO content is 0.05–0.27 wt% (on average 0.11 wt%).

Cr-bearing diopsides are present in almost all magmatic bodies of the Chompolo field, with the exception of Intrusion 104. The studied Cr-diopsides can be combined into a large group (II; see Figure 4) with a characteristic $\text{Ca}/(\text{Ca} + \text{Mg})$ ratio ranging between 48 and 52 and a high Cr_2O_3 (0.8–4.34 wt%) and Al_2O_3 (0.80–8.9 wt%) content relative to the group I Cpx (Table S2). Group II Cpx are also characterized by a wide range of $\text{Mg}/(\text{Mg} + \text{Fe}_{\text{tot}})$ molar ratios in the limits of 0.79–0.96 where the average value of 1030 analyses is 0.94. The diopsides also contain low amounts of TiO_2 , up to 0.47 wt% (on average 0.11–0.16 wt%). The group II Cpx are characterized by a negative correlation of $\text{Mg}\#$ with Na_2O and Al_2O_3 . In group II, the Na_2O content was higher (0.33–4.96 wt%) and MnO was relative to group I Cpx.

4.3.4. Mica

Minor amounts of mica occur in the Sputnik pipe and the Aldanskaya dyke: up to 2-mm euhedral grains of phlogopite to siderophyllite minerals (Table S3). Mica microphenocrysts have a composition with high Al_2O_3 (13.1–16.8 wt%) and especially FeO (8.3–21.6 wt%) contents, a wide range of TiO_2 (1.7–5.5 wt%), with 0.1–0.6 wt% BaO, 0.3–1.7 wt% F and up to 1.1 wt% Cl (Figure 5).

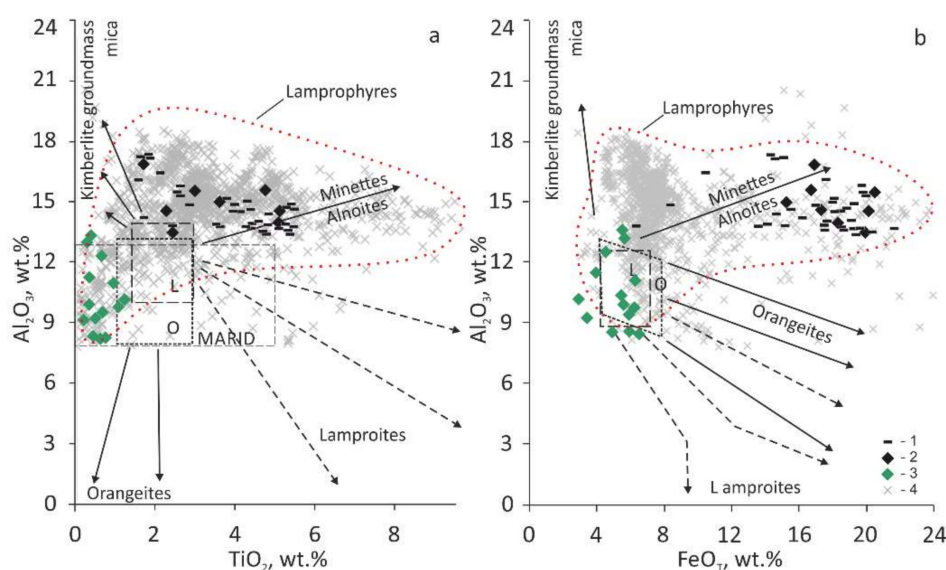


Figure 5. Al_2O_3 vs. TiO_2 (a) and FeO_T (b) in micas from Sputnik pipe (1), Aldanskaya dyke (2) and mica inclusions in Cpx rims from the Aldanskaya dyke (3); blocks mark compositions of orangeite (O)

and lamproite (L) microphenocrysts and evolutionary trends based on [53–55]; field of lamprophyres are shown according to [27]. This covers the majority of published mica compositions from lamprophyres (4, n = 1310); the Geochemistry of Rocks of the Oceans and Continents (GEOROC) database (<http://georoc.mpch-mainz.gwdg.de>) was used.

The phlogopites included in the rims of zoned clinopyroxenes from the Aldanskaya dyke (Figures S1 and 5) are characterized by relatively high MgO content (23.0–25.1 wt%), lower Al_2O_3 (9.4–13.5 wt%) and not a very wide range of TiO_2 (0.3–1.2 wt%) (Table S3).

4.3.5. Amphibole

The amphiboles are mainly of Ti-K-pargasite-edenite varieties with minor Fe-chermakite, Mg-gastingsite, and Mg-hornblende. They have 0.7–3.3 wt% TiO_2 with high Mg# 0.81–0.96. The contents of K_2O vary from 0.3 to 2.5 wt% (Figure 6b, Table S4).

K-richterite crystals are transparent, greenish-yellow, regularly shaped 1–2-mm platelets without visible zoning. The amphiboles from a non-oriented sample of the Aldanskaya dyke show Raman shifts in perfect accordance with K-richterite XIII-83/5 from the Geological Museum of the Institute of Geology and Mineralogy (Novosibirsk) (Figure S3) and with the standard R060034 from the RRUFF database [44].

The analyzed K-richterite samples (Table S4) show low amounts of TiO_2 (0.05–0.12 wt%), Cr_2O_3 (0.07–0.26 wt%), and Al_2O_3 (<0.48 wt%), minor amounts of F (<0.34 wt%), and high Na/K = 1.2–4.3. K_2O contents vary from 1.2 to 5.07 wt%, while FeO_T and Na_2O remain relatively constant (1.9 ± 0.25 wt% and 4.1 ± 0.44 wt% on average, respectively) (Figure 6a).

4.3.6. Apatite

Based on the concentration of Sr, F, Cl and the sum of other REE elements (Nd, Ce, La, Pr), the apatites can be divided into three varieties (Table S5). The first variety is characterized by a low concentration of REE elements (0.1–1.7 wt%) and elevated volatile contents (F + Cl) that reach 1.9–4.6 wt%. The second variety of apatite is the most prevalent and is characterized by a slightly elevated concentration of REE elements (0.42–2.9 wt%) and decreased volatile contents (F + Cl) that vary within the range of 0.6–1.55 wt%. Six grains belong to a high-Sr variety of apatite with a concentration of SrO in the range of 4.5–15.6 wt% and low volatile contents (F + Cl = 0.53–0.97 wt%).

4.3.7. Garnets

The garnets were classified into paragenetic types in accordance with the existing scheme for mantle-derived garnets [56,57], including screening them from crustal varieties. Mantle garnets prevail in the Aldanskaya dyke and in the Sputnik, Gornaya, and Ogonek pipes, while crustal and eclogitic garnets dominate in the Perevalnaya and Kilier-East pipes (Table 2).

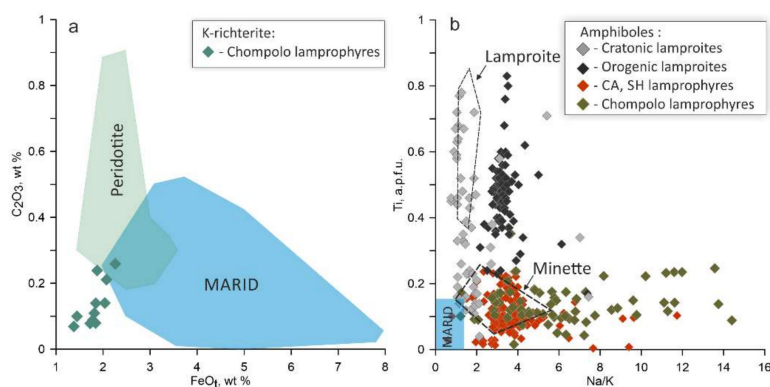


Figure 6. Cr_2O_3 (wt%) vs. FeO_T (wt%) in K-richterite from Aldanskaya dyke; fields for K-richterite

from mica–amphibole–rutile–ilmenite–diopside (MARID) and peridotite samples are shown based on [58] and references therein (a). Ti–Na/K (expressed as a.p.f.u.) variations in amphibole compositions in lamprophyres of Chompolo field, calc-alkaline (CA) and shoshonitic lamprophyres [59–63], cratonic [5,64–72] and orogenic lamproites [73–76] (b). Minette, lamproite and mica–amphibole–rutile–ilmenite–diopside (MARID) fields modified from [54].

Table 2. Genetic types of garnets from the Chompolo dikes and pipes (%).

Object	n	UC	LC	E	DE	LPL	HPL	HTL	W	HD
Sputnik	140	1.2	4.0	5.8	0.6	70.4	9.8	6.9	1.2	0.1
Ogonek	317	4.2	6.9	7.8	0.2	60.3	15.9	1.2	0.2	3.2
Gornaya	323	6.4	10.8	7.8	2.3	51.1	18.6	0.9	0.7	1.4
Aldanskaya	260	5.3	12.2	11.4	0.3	46.5	22.4	0.8	0.0	1.1
Kilier-East	18	33.7	32.0	18.5	0.0	10.7	5.1	0.0	0.0	0.0
Perevalnaya	131	25.8	71.9	2.3	0.0	0.0	0.0	0.0	0.0	0.0
Intrusion 104	116	95.2	4.8	0.0	0.0	0.0	0.0	0.0	0.0	0.0

Numbers correspond to types of garnets derived from: upper crust (UC); lower crust granulite (LC) [77]; eclogite (E); potentially diamondiferous eclogite (DE); LP lherzolite (LPL); HP mantle lherzolite (HPL); HT lherzolite (HTL) [78,79]; wehrlite (W); and harzburgite–dunite (HD) [57]. Megacrysts garnets were not found [80].

The peridotitic garnets from the Chompolo alkaline rocks, with a total number of 1040 analyses, are depicted in the CaO–Cr₂O₃ diagram (Figure 7, Table S6). All garnets are chromium pyropes with Cr₂O₃ content from 0.5 to 9.92 wt% and Mg# in the range of 0.62–0.86. However, the majority of pyropes (73%) are characterized by a narrower range in Mg# (0.77–0.81). The CaO content varies between 1.85 and 10.29 wt%, and TiO₂ does not exceed 0.47 wt%. The pyropes are enriched with MnO with values usually more than 0.4, up to 1.29 wt%.

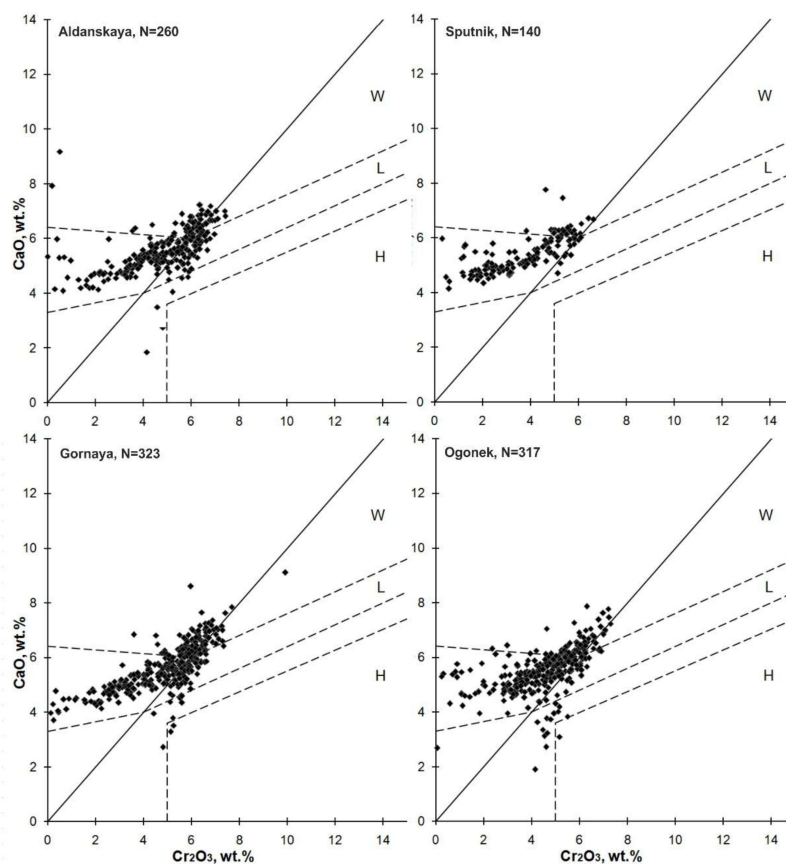


Figure 7. Cr₂O₃ (wt%) vs. CaO (wt%) correlation in pyrope garnets from Aldanskaya dyke and

Sputnik, Gornaya, and Ogonek pipes [57]. Letters stand for parageneses: H = harzburgite–dunite, L = lherzolite, W = wherlitolite.

The pyropes can be characterized by paragenetic types according to the CaO–Cr₂O₃ discrimination diagram. Most of the mantle garnets are lherzolitic (Figure 7), with more abundant low-pressure lherzolite varieties and some high-pressure lherzolite garnets containing up to 10 mol% of knorringite. The population of mantle garnets includes small percentages of dunite–harzburgite and wehrilitic garnets but lacks megacrystalline and high-temperature lherzolitic varieties common to kimberlites, as well as subcalcic high-Cr varieties. The abnormal character of the composition of these pyropes is expressed in a distinct trend of partitioning their compositions on the Cr₂O₃–CaO discrimination diagram. The discrepancy stems from a different ratio of Cr₂O₃ and CaO contents, owing to the high-Cr part of the trend falling on the field of wherlitolite garnets.

4.3.8. Cr-Spinel

We analyzed Cr-spinels that were 0.2–2 mm macrocrysts (over 1000 grains), selected from the heavy mineral concentrates of five bodies (Table S7). The content of major oxides in Cr-spinels (Figure S4) varies within broad ranges (3.5–50.9 wt% Al₂O₃, 18.6–63.5 wt% Cr₂O₃, and 6.1–19.1 wt% MgO). They, likewise, have large ranges of Cr# as molar $100 \times \text{Cr}/(\text{Cr} + \text{Al})$, from 20 to 86, and are characterized by a close negative correlation between Cr and Al (Figure S4). The ratio $100 \times \text{Fe}/(\text{Fe} + \text{Mg})$ (Fe#) also varies broadly from 23.7 to 69.5. The TiO₂ content in most spinels is below 0.5 wt% with a maximum of 1.6 wt%. The spinel populations from different bodies have generally similar compositions with Cr₂O₃ being the highest in those from the Ogonek and Sputnik pipes and the Aldan dyke (63.5, 63.2, and 62.6 wt%, respectively), which is commensurate with Cr₂O₃ in diamond-related spinels [81].

Spinel included in the rims of zoned clinopyroxene are characterized by high FeO content (Figure S1).

4.3.9. Ilmenite

Ilmenites from the Aldanskaya dyke are of two main chemical types (Table S8), one being more magnesian MgO (4.6–11.2 wt%) and containing more MnO, Cr₂O₃, NiO (0.3–0.7, 1.4–2.3, 0.14–0.21 wt%, respectively) and Al₂O₃ than the other. Another type of ilmenite occurs in the Gornaya, Ogonek and Perevalnaya pipes, hemoilmenite, which contains up to 90.5 mol% ilmenite, 9.9 mol% geikelite, and 35.5 mol% hematite components, with relatively high amounts of Al₂O₃ and Cr₂O₃ (0.3 and 1.08 wt%, respectively). Hemoilmenite with such a composition is known from African [82,83] and Yakutian kimberlites [84].

4.4. Geochemistry

As mentioned above, the rocks are characterized by different degrees of post-emplacement modifications, carbonization and hydration, which is reflected in the high LOI values for most of samples. Thus, it is reasonable to take into account, with accuracy, the CaO and MgO oxides (decreased MgO and elevated CaO concentrations in some samples), as they have undergone apparent weathering reactions to the relatively inert TiO₂ and P₂O₅ oxides (Table S9).

4.4.1. Major Elements

The Chompolo rocks are ultrapotassic with high K₂O (1.8–5.5 wt%) (Figure 8a, low Na₂O (0.2–1.4 wt%), and high K₂O/Na₂O ratio (up to 26, mostly 2.5–7). Silica content is higher for Intrusion 104 rocks (54 wt% SiO₂) in comparison with Aldanskaya and Ogonek rocks, which have lower silica content (mostly 38–50 wt% SiO₂). All samples in most cases have high Mg# = molar Mg/(Mg + Fe), ranging from 0.65 to 0.85, with some exceptions for samples with elevated CaO and reduced MgO amounts due to post-magmatic alteration (Table S9). High concentrations of Al₂O₃ (7.2–12.8 wt%) in the rocks results in sub-unity values of $(\text{K}_2\text{O} + \text{Na}_2\text{O})/\text{Al}_2\text{O}_3 = 0.4\text{--}0.7$. Taking into account their low

sodium concentrations, in the K_2O/Al_2O_3 vs. SiO_2 diagram (Figure 8b), the studied rock samples are plotted onto the field of the Roman-type ultrapotassic magmas based on Foley et al. [85]. Concentrations of TiO_2 and P_2O_5 are low and vary in the ranges of 0.4–0.7 wt% and 0.1–0.9 wt%, respectively.

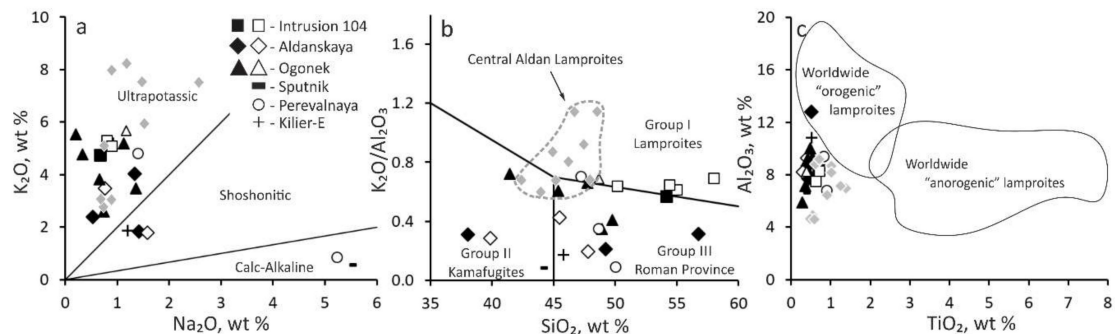


Figure 8. K_2O vs. Na_2O diagram [85] (a); bold line dividing alkaline and subalkaline rock series based on [86]; major element variation diagrams of K_2O/Al_2O_3 vs. SiO_2 for ultrapotassic rocks subdivided into three main groups: group I lamproites, group II kamafugites and group III Roman Province, based on [85] (b); Field for Central Aldan lamproites plotted according to [11]. Al_2O_3 vs. TiO_2 diagram for the Chompolo rocks (c); filled black symbols are data from this work and empty symbols are data from [25]; data for worldwide orogenic and anorogenic lamproites (data from [87] and references therein) are reported for comparison.

4.4.2. Trace Elements

The primitive mantle-normalized (PM-normalized) multi-element patterns and chondrite-normalized rare earth element (REE) patterns of the Chompolo rocks are plotted in Figure 9a,b along with group I kimberlites [87], Leucite Hills lamproites [88] and Central Aldan lamproites [11]. The analogous element patterns for lamprophyres and minettes from Canada, USA and China [89–93] are plotted in separate figures (Figure 9c,d).

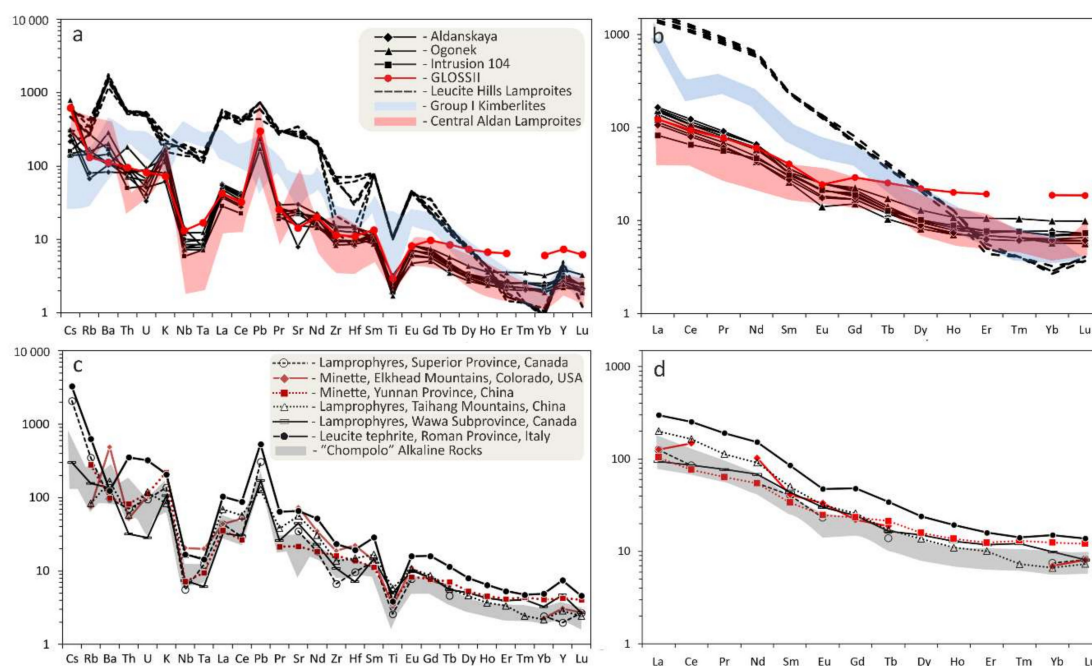


Figure 9. Primitive mantle (PM)-normalized trace element abundances (a,c) [94], and chondrite-normalized rare earth element (REE) patterns [95] in Chompolo rocks (solid black line) (b,d). (a) Chompolo rocks together with lamproites from Leucite Hills (black dash line), according to [88]; group I kimberlites (blue

field), according to [87]; Aldan lamproites (red field), according to [11]; (b) lamproites from Leucite Hills (black dash line), according to [88]; group I kimberlites (blue field), according to [87]; Aldan lamproites (red field), according to [11]; (c) representative CA and shoshonitic lamprophyre patterns from Canada, USA and China compared with the range of Chompolo alkaline rocks (shaded field) (data sources: [89–93]); (d) CA lamprophyres from Taihang Mountains, north China (blue dash line), according to [90]; generation I (black dotted line) and generation II (red dotted line) minettes from Yunnan Province, China [89]; CA and shoshonitic lamprophyre patterns from Canada [91,92].

Obviously, the multi-element and rare earth element patterns of the Chompolo rocks are almost equivalent to the “Aldan lamproites” and fit very closely with the minettes.

The degree of trace element enrichment of the Chompolo rocks and “Aldan lamproites” is up to an order of magnitude less than that of other lamproites (Figure 9a). The Chompolo PM-normalized multi-element patterns are characterized by high enrichment in large-ion lithophile elements (LILE: Rb, Ba, Cs), sharp troughs in some high field strength elements (HFSE: Ti, Nb, Ta), as well as high Pb concentration. The rocks also show a low fluctuation of Zr and Hf and a lower concentration of strontium relative to “Aldan lamproites”. The La/Nb and K/Nb ratios for the Chompolo rocks are higher than for most known lamproites and lamprophyres and are commensurate with those for the “Aldan lamproites” (Figure 10a). Compared to typical kimberlites and lamproites, Chompolo rocks have low $(\text{La/Yb})_N$ ratios (17.3–39.3) and a weak Eu anomaly, with Eu/Eu^* ratios of 0.81–0.96 (Figure 9b).

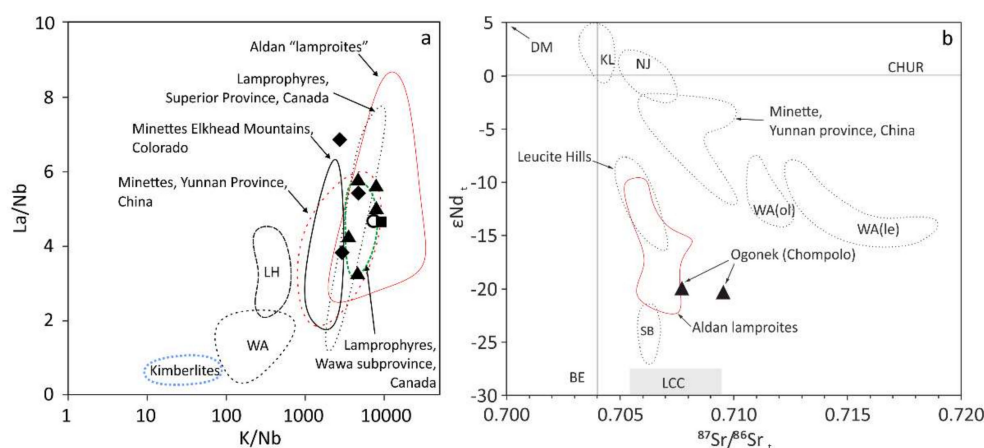


Figure 10. Variations in K/Nb versus La/Nb for Chompolo rocks (a) and ϵNd_t vs. $^{87}\text{Sr}/^{86}\text{Sr}_t$ for lamproite (lamprophyre) occurrences of Aldan shield with new data for the Chompolo alkaline rocks (b). For comparison, the fields for kimberlites, lamproites and lamprophyres are given. Abbreviations correspond with kimberlites (KL), Western Australia olivine WA (ol) and leucite WA (le) lamproites, Leucite Hills lamproites (LH), Navajo volcanic field (NJ), Smoky Butte (SB). Description for symbols given in Figure 8. Data sources for (b): [11,53,96,97].

4.4.3. Nd–Sr Isotopes

Sr and Nd isotopic ratios for the Ogonek pipe are reported in Table S10 and plotted in Figure 10b. Initial isotope ratios were calculated, accepting 138 Ma as the emplacement age. The initial $^{87}\text{Sr}/^{86}\text{Sr}$ ratios are 0.70954 and 0.70775, whereas the initial $^{143}\text{Nd}/^{144}\text{Nd}$ ratios are 0.51150 and 0.51163 with unradiogenic ϵNd_t values of -20 on the ϵNd_t versus $^{87}\text{Sr}/^{86}\text{Sr}_t$ plot (Figure 10b).

Both isotope systems have compositions that correspond to the most-evolved end of the mantle reservoir that has undergone a long-term process of Light Rare Earth Element (LREE) enrichment and moderate Rb/Sr enrichment. The model age values obtained for the Ogonek pipe samples, calculated relative CHUR (T_{CHUR}) and depleted mantle (T_{DM}) yield—1926 Ma and 2350 Ma, respectively.

The difference between Rb, Sr, Sm and concentrations obtained by ICP-MS and isotope dilution for the Og-5 sample (Tables S9 and S10) is possible due to the varies of crustal rock clasts in aliquots analyzed by ICP-MS and the isotopic technique. A relatively high radiogenic $^{87}\text{Sr}/^{86}\text{Sr}$ ratio of the Og-4 sample is outside of the common intraplate lamprophyre values, and Aldan alkaline complexes, in particular. This indicates the Sr isotopic disequilibrium and Sr loss of this sample that is related to a postmagmatic alteration.

5. Discussion

5.1. Geochronology

There much interest in obtaining the emplacement ages of the Aldanskaya and Ogonek magmatic bodies due to their better accessibility for studies. As mentioned above, there is published research that identifies a Rb-Sr Early Cretaceous age for the Intrusion 104 body [39]. Unfortunately, the Rb-Sr isochron method is very sensitive to weathering processes [98] and thus it is better to use a method that is insensitive to the hydrothermal alteration of the rocks whenever possible. The rocks also contain some zircon grains, but these obviously have a crustal origin based on their size, morphology and very old age (older than 1700 Ma, unpublished data). Other minerals suitable for the U-Pb dating method have not yet been found in the Chompolo rocks.

Despite the difficulties, we were able to find K-amphiboles that be used to date the rocks. The results of the age determinations for the Ogonek pipe (137.8 ± 1.2 Ma) and the Aldanskaya dyke (157.0 ± 1.6 Ma) were obtained using the ^{40}Ar - ^{39}Ar method of dating the K-richterites and demonstrated uniform plateau ages from the argon-release spectra (Figure 3). The significant difference in the Ar-Ar ages of K-richterites from the Ogonek pipe and the Aldanskaya dyke can be explained by several pulses of magmatism. That is clearly seen in the geological structure of the Ogonek pipe, which is complicated by a 250-meter-long dyke. The age-related relationships between diatreme and dyke are unknown. The resulting ages correspond to the Mesozoic stage of alkaline magmatism that occurred widely within the Aldan shield.

5.2. Xenocrysts as Evidence of the Deep Mantle Source of the Rocks

There is some evidence that relatively MgO-poor rocks can bear mantle xenolith or xenocrysts. Among the earlier published evidence, the fact that that xenolith-bearing lamprophyres were fractionated after xenolith incorporation was published by Wright [99]. An abundance of mantle-type ultramafic xenoliths (lherzolites, harzburgites) and xenocrysts (interpreted as a product of xenoliths disintegration), as well as eclogite xenoliths, in a variety of lamprophyres, were reported in the overview by Rock [85]. In particular, xenoliths of garnet-bearing peridotites and xenocrysts of mantle minerals were recorded in minettes of the Navajo volcanic field [100]. Post-Archean calc-alkaline lamprophyres (minettes and spessartites) of the Wawa and Abitibi subprovinces (Canada) bear ultramafic xenoliths and microdiamonds [91].

A feature of Chompolo rocks is the presence of xenocrysts of minerals that originate from the lithospheric mantle. However, mantle xenoliths that are common in kimberlites were not found in the Chompolo rocks, in contrast to the intergrowths of pyropes and clinopyroxenes that occurred regularly. All other occurrences of alkaline magmatism within the Aldan alkaline province, including lamproites of the Yakokut complex, Ryabinovyi, Murun and Lomam complexes, the Molbo dyke, rocks of the Tobuk–Khatystyr field (with the exception of the Yagodka pipe) and others (Figure 1) [11,13,14,17,101,102], are devoid of garnet-bearing mantle xenoliths and xenocrysts of pyrope garnets and probably originated from shallower depths.

The compositional features of the investigated pyropes, Cr-spinels and clinopyroxenes indicate the dominance of spinel and garnet–spinel lherzolites in the mantle section, while minerals of garnet lherzolites, dunites, harzburgites and eclogites are less abundant. PT estimates of the lithosphere based on thermobarometric mineral methods show values of 2.9–3.6 GPa and temperatures of 710–770 °C [103].

However, these estimates have been made for a limited sample collection of mantle pyropes with inclusions. Previous estimations based on single-mineral thermobarometry of Cpx, Opx and pyropes demonstrate the same range of 2.0–4.2 GPa for pressure [104].

5.3. Rock Classification Based on Mineralogical Features and Whole-Rock Chemistry

The affiliation of the Chompolo rocks with the lamprophyres is based on mineralogical and geochemical criteria summarized in the second edition of the subcommission recommendations of the International Union of Geological Sciences (IUGS) on the systematics of igneous rocks [105].

The Chompolo rocks were originally classified as kimberlites for their typical mantle mineralogy comprised of pyrope, Cr spinel, and Cr diopside [19,22–24]. Although Chompolo igneous rocks contain xenocrysts of mantle minerals, their mineral and chemical composition clearly indicate that they are not kimberlites [105]. Alkaline volcanic rocks commonly have a large variation in concentrations of major oxides [106,107]. This compositional diversity is due to fractional crystallization upon magma ascent, contamination, the incorporation of xenogenic material, and hydrothermal–metasomatic processes [87,108]. The Chompolo rocks underwent secondary alteration processes as well. The ratio of major oxide concentrations and the LOI demonstrate that, in the studied rocks, the CaO and, in some cases, MgO concentrations were modified. These changes are caused by the replacement of magnesium and calcium silicates (olivine, clinopyroxene) by secondary minerals under the influence of CO₂-enriched aqueous solution. As a consequence of these processes, in some cases (Ald-3, Table S9) elevated silica concentrations are also observed. For this reason, the aforementioned elements cannot be discussed further.

The ultrapotassic character of the Chompolo rocks (K_2O/Na_2O is mostly 2.5–7) matches that of lamproite, but does not align with the compositional criteria of typical lamproite, which is characterized by a molar ratio of $K_2O/Al_2O_3 > 0.8$ and $(K_2O + Na_2O)/Al_2O_3 > 1$, according to [105,109]. In addition, the low TiO₂ and relatively lower Ba, Sr, Zr, and La contents of the rocks are not typical for lamproites [105]. In fact, the PM-normalized trace elements pattern and chondrite-normalized REE of Chompolo rocks are similar to those of the Central Aldan lamproites and Chinese lamprophyre and minettes [89,90]. However, the rocks should not be defined solely by their whole-rock chemistry and, in this respect, chemistry in combination with mineral composition features establishes more reliable criteria to properly identify the affinity of the Chompolo rocks. Mineralogy (Table 1) and chemistry (Table S9), as well as the textural and structural features of alkaline igneous rocks of the Chompolo field, can be summarized as follows. These rocks form veins or dykes and volcanic pipes that are characteristic of lamproites or lamprophyres and are characterized by a medium- to fine-grained porphyritic texture. The micro- to crypto-crystalline matrix consists mostly of sanidine and products of its chemical weathering, such as micas, chlorite, and minor opaque minerals. The matrix encloses micro-phenocrysts and some altered olivine, sanidine, mica (Fe- and Al-rich phlogopite-siderophyllite), apatite and amphibole (pargasite-edenite) phenocrysts. The presence of small amounts of carbonate minerals is due to secondary hydrothermal processes and the rocks bear signatures of carbonation and silicification (Ogonek and Perevalnaya pipes).

The cognate mineralogy of the Chompolo rocks comprise olivine, sanidine, mica, clinopyroxene, amphibole and accessory minerals like apatite. The K-feldspar (sanidine) are represented both as phenocrysts and as a matrix mineral component. Minor to trace amounts of Ba and Fe₂O₃ in the K-feldspar composition, along with Na-K-Ba within-grain zoning, are characteristic of the lamprophyre series of rocks [110]. Low Na₂O and CaO concentrations at variable Fe₂O₃ are also typical of K-feldspar from lamproites [54] and orangeites [53]. Matrix K-feldspar with an Fe₂O₃ impurity is common to minettes [27].

The mica is compositionally proximal to those from calc-alkaline (CA) lamprophyres (minettes) and ultramafic (UM) lamprophyres (alnoites), which show high Al₂O₃ and FeO and broadly varying TiO₂ contents (Figure 5). Phlogopites with the composition described for the Chompolo rocks are common to all lamprophyre varieties but strongly differ from lamproite micas, which show significantly lower Al₂O₃ [105,111].

A lamproite designation could be supported by some aspects of the Chompolo mineralogy, for example the Al- and Na-depleted clinopyroxene (augite) (<1 wt% Al_2O_3 and <1 wt% Na_2O), but a similar composition of clinopyroxene is also typical for CA lamprophyres [110]. Although K-richterite is one of the diagnostic minerals of lamproites, it may also be present in lower quantities in CA lamprophyres. As for the K-richterite restricted to the Ogonek pipe and Aldanskaya dyke, it has a low TiO_2 concentration that is more typical of amphiboles of CA lamprophyres [110]. K-richterites from the Chompolo rocks are compositionally proximal to alkaline amphiboles from the Bohemia minettes [112] and the Yinniugou ultramafic lamprophyres [113]. The xenogeneic origin of K-richterites in the Chompolo lamprophyres is also possible. K-richterites are found in mantle peridotites and the mica–amphibole–rutile–ilmenite–diopside (MARID) suite and can be a metasomatic phase [58], taking into account the evidence of mantle metasomatism recorded in pyropes from the Chompolo lamprophyres [103,114]. However, the composition of K-richterites from the Aldanskaya dyke has obvious differences—lower FeO and Cr_2O_3 contents relative to K-richterite from peridotites and the MARID suite (Figure 6a). Mica are not MARID in composition either (Figure 5), while rutile is rare and ilmenite is almost absent.

Ca-amphiboles (Ti-K-pargasite-edenite), which are a characteristic mineral in CA lamprophyres, and are almost absent in lamproites [27], are more widely represented in the studied rocks from the Sputnik pipe and Aldanskaya dyke. Amphiboles of lamproites and calc-alkaline (and shoshonitic) lamprophyres are easily distinguishable in terms of their Ti vs. Na/K ratio. For comparison, the groups of aforementioned amphiboles from well-known occurrences are plotted on the Ti vs. Na/K (as a.p.f.u.) discrimination diagram (Figure 6b).

Apatite is an accessory mineral that commonly occurs in different types of alkaline rocks. Impurities of SiO_2 are typical for kimberlitic apatite [115–117]. Significant SiO_2 concentrations (up to 3.61 wt%) are recorded in Kasma 45, and Kasma 47 archetypal kimberlites, and the Kuusamo Area [118]. Compositionally similar F apatite with SrO more than 1 wt% is common for lamproites [53], but apatite in the latter category usually contains 0.2–0.4 wt% to 18 wt.% BaO [53], which is absent in the Chompolo samples.

There are no ‘forbidden’ minerals for lamproites in Chompolo rocks, but typical lamproite minerals, such as leucite or Ba-Ti-Zr-bearing minerals (priderite, wadeite, lindsleyite, etc.), are also absent. The studied rocks fit all the main criteria for the identification of a rock in the lamprophyre series: the mineral and chemical composition of the rocks, the texture, the form of the geological bodies, and the specific chemical composition of rock-forming minerals.

Based on petrographic, mineralogical and geochemical data, the studied rocks definitely belong to lamprophyres according to the published criteria [105,109,119,120]. Mineralogically, these rocks are closer to minettes with their potassic feldspar and phlogopite in the matrix. A more precise classification of the Chompolo rocks is difficult, which can be explained by heteromorphism [27]. According to the provided “equations” [27], the mineral assemblages in minettes, vogesites, kersantites and spessartites can form in chemically equivalent magmas with the final mineral assemblage dependent on the local emplacement conditions.

5.4. Isotopic and Trace Element Data

According to their significantly unradiogenic Nd isotope composition ($E_t = -20$) and moderately radiogenic Sr isotope composition (0.7077, 0.7095), the source of the Chompolo rocks corresponds to an enriched mantle reservoir that has been isolated from the convective asthenosphere for a long time prior to melt formation. The unradiogenic Nd ($E_t =$ down to -25) and moderately radiogenic Sr isotopic compositions (0.70499–0.70822) are typical of Aldan shield alkaline complexes like Tommot, Lomam, Ryabinoviy, Yakokut, Murun, Bilibinskiy, and Khani [10,11,121,122]. Close Sr–Nd isotopic ratios of the Chompolo rocks and “Aldan lamproites”, including aforementioned alkaline complexes, evidenced that they derived from the same mantle reservoir.

Most lamproites worldwide show minor HFSE depletion relative to elements with similar degrees of incompatibility. Overall, the HFSE, Th, U and LREE display unusually low concentrations for lamproites

or kimberlites. The PM-normalized trace element pattern and chondrite-normalized REE of Chompolo rocks are close to those of the Central Aldan lamprophyres and Chinese lamprophyres and minettes [89,90].

The characteristic trace element composition of the Chompolo rocks with enrichment in LILE and LREE alone, and with negative Nb-Ta and Ti anomalies in the PM-normalized trace elements diagram are indicative of an origin from a source affected by a water-rich metasomatic agent [123,124]. In general, the above-mentioned anomalies and the peak in Pb make the trace element distribution very similar to global subducting sediments (GLOSSII, [125]; see Figure 9). Pearce [126] showed the tendency of Th to concentrate in the continental crust relative to Nb and Ta, which are generally depleted. This element's behavior can be used for understanding crustal contributions in volcanic rocks' petrogenesis. The lines of equal Th/Nb ratio are shown on the Th/Y versus Nb/Y diagram (Figure 11a) that also contains average points of the lower and upper crust [127], as well as GLOSSII in [125]. Mantle arrays are characterized by a restricted range of the Th/Nb ratio (<0.17) relative to crustal rocks, which have a significantly higher Th/Nb ratio (up to 1.9) [96]. The high Th/Nb ratio of the Chompolo rocks suggests crustal involvement in the mantle source, especially close to the upper continental crust (UCC) or GLOSSII in terms of the Th/Nb ratio. The lower continental crust has lower Th/Nb ratios than the Chompolo rocks; nevertheless, it cannot be excluded from the mixing end member for a relatively more Th-enriched mantle source. Relatively high Th/La (0.20–0.42) and high Ba/Nb (75–329) ratios and low Sm/La (0.12–0.23) and Ce/Pb (3.1–4.6) ratios confirm that the mantle source was modified by a crustal component (Figure 11b). The occurrence of the crustal component is also supported by a wide distribution of Paleoproterozoic zircon grains and crustal garnets (Table 2) in the studied intrusions.

A widely used model of shoshonite–calc-alkaline lamprophyre genesis—suggests a metasomatized subcontinental lithosphere mantle (SCLM) source that has been enriched by H₂O-bearing fluids released from an ancient subducted oceanic crust with (terrigenous/pelagic) sediment contributions [128–130]. In this way, contamination by the continental crust cannot be discounted; nevertheless, the Chompolo rocks have relatively high Mg# = 0.65–0.68. In addition, the Nb/U ratio of the Chompolo rocks (3.6–10.3) is significantly less than the values for midocean ridge basalts or ocean island basalts (OIB) (Figure 11c). On the Nb/U vs. Nb diagram the Chompolo rocks' values are located below or opposite the field of the continental crust values, suggesting that the enrichment of U relative to Nb could not be produced by a simple mixing of mantle and crustal sources.

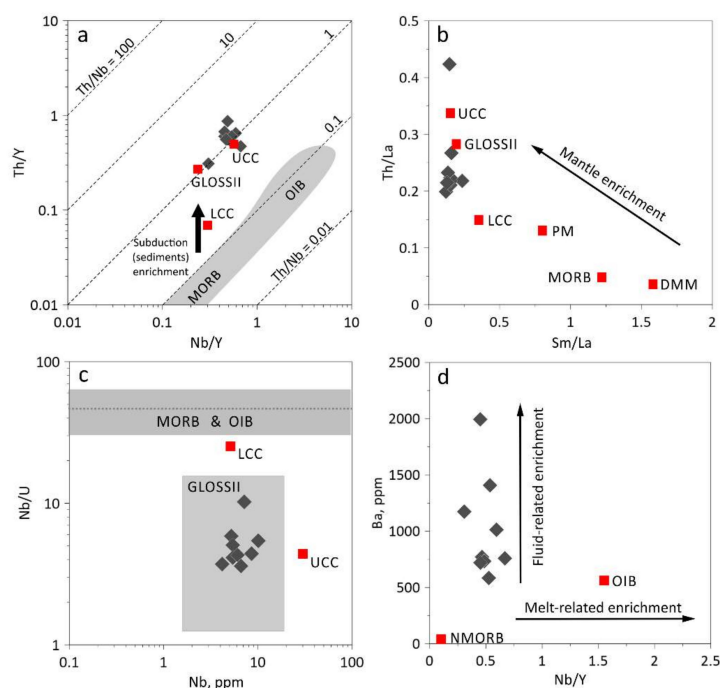


Figure 11. Discrimination diagrams for Chompolo rocks: (a) Th-Nb proxy for crustal input diagram

based on [96]; (b) variations in Th/La versus Sm/La based on [131]; (c) Nb/U versus Nb (ppm) plot based on [132]; (d) Ba (ppm) versus Nb/Y plot for Chompolo rocks based on [133]. Data sources: upper continental crust (UCC), lower continental crust (LCC) from [127]; global subducting sediments (GLOSSII) from [125]; primitive mantle (PM) and midocean ridge basalts (MORB) from [134].

However, it is easy to see that the Nb versus Nb/U ratio for Chompolo rocks is located within the GLOSSII field, suggesting the contribution of a sediment-rich source. The melt, produced by experimental modelling of a 10% melting of modified GLOSS [135], demonstrates the same geochemical features (i.e., enrichment in the highly incompatible elements, negative Ta-Nb and positive Pb anomalies, and less pronounced relative depletion in Zr and Hf) that are observed in the studied Chompolo rocks. Bulatov et al. [135] concluded that these features of the partial melts are merely inherited from the geochemical signature of the GLOSS composition.

It was shown experimentally that Sr and Ba are more soluble in aqueous fluid than REE at high P and T conditions [136]. The contribution of a LILE-enriched aqueous fluid can be evaluated from Sr/Nd and Ba/La ratios, which should be high (i.e., >17 and >40, respectively) [137–139]. In the Chompolo rocks, relatively high ratios of Sr/Nd (with the majority in the range of 16–25) and Ba/La (19–60) are observed, which confirms the LILE addition to the ancient mantle source by an aqueous-rich metasomatic agent. The trend shows Ba increasing at a constant Nb/Y ratio, which also indicates a fluid-related enrichment of the mantle source (Figure 11d).

High K₂O contents, as well as a positive correlation of La/K and La/Ba ratios with La that was exhibited by the Chompolo rocks (Table S9), suggest that a potassic phase is present in the mantle source region [140]. Such a mantle reservoir has to contain K-bearing phases, such as mica or amphibole, to be a source of potassic magmatism. Melts in equilibrium with phlogopite are expected to have an Rb/Sr ratio higher than 0.05, and a Ba/Rb ratio lower than 30 [141,142]. The Chompolo rocks demonstrate ranges of 0.07–0.37 for Rb/Sr ratios and a range of 6.8–23.4 for Ba/Rb ratios that are more consistent with a mantle source containing phlogopite. Additional evidence of metasomatic processes in the mantle source of the Chompolo rocks is the broad positive correlation between Zr and K (Ba) that point toward a Zr-bearing phase (crichtonite group minerals) that is associated with phlogopite and potassic amphiboles [143,144]. Low TiO₂ content in the rocks along with a high Nb/Ta ratio with respect to the primitive mantle indicate the presence of a Ti-rich phase (rutile or amphibole) in the mantle source that has remained in the residue during partial melting, as also indicated by the negative Ti anomaly on the PM-normalized trace element patterns.

All this evidence supports the formation of an enriched mantle source of Chompolo alkaline rocks under the effect of two combined processes related to the partial melting of recycled crust and the infiltration of aqueous fluids released from subducted crustal material. In the case, if there was significant sediment partial melting, the mantle source would not have a suitable composition to produce alkaline magmas due to the fact that such partial melts are too SiO₂ rich. The peculiarities of trace element distribution also suggest that the partial melting was not the major factor that controlled the enrichment processes of the mantle source of the Chompolo rocks. LILE and LREE elements are mobile and enrich the mantle source with the help of an aqueous-rich metasomatic agent released from a subducted slab. This type of metasomatic process is required by the geochemistry of the Chompolo rocks and their mantle-derived xenocrysts as well.

5.5. Metasomatic Mineral Assemblages in the Pyropes from the Central Aldan SCLM

Mineral assemblages in the pyropes from the Central Aldan subcontinental lithospheric mantle (SCLM) were described previously in separate studies [103,114,145,146]. The composition of mineral inclusions in lherzolitic and harzburgitic Cr-pyropes from the Aldanskya dyke and Ogonek pipe is evidence of metasomatic mineral associations in the mantle under the Aldan shield. Garnet xenocrysts from the Chompolo rocks host mineral inclusions enriched in volatile (e.g., carbonates, mica and amphibole) and incompatible trace elements (e.g., crichtonite group minerals, Nb-rutile and mica).

These garnets enclose graphite coexisting with forsterite, diopside, Ba-Cl-phlogopite, tschermakite, rutile, magnesiochromite, Mg-ilmenite, apatite, chalcopyrite, dolomite, magnesite and lindsleyite inclusions [28]. The parental peridotites were interpreted as fragments of the lithospheric mantle, which was metasomatized by C-bearing fluids derived from a paleosubduction slab. Obviously, the magmatic source of the initial melts of the lamprophyres has to come from below the metasomatized region of the SCLM to capture the mantle xenocrysts. On the other hand, these events—the SCLM metasomatism and the Mesozoic stage of alkaline magmatism—could be distant in terms of time.

5.6. Geodynamic Implications

According to the discrimination diagram based on the compilation of Lustrino et al. [147], it is evident that alkaline rocks of the Aldan shield, including ‘Russian lamproites’, have similar values of Al_2O_3 and TiO_2 , like orogenic lamproites worldwide (Figure 8c). Nevertheless, their position on the diagram is distinctive from the field of typical ‘orogenic lamproites’ because of their decreased TiO_2 and Al_2O_3 contents. As shown by Vollmer [9] and Nelson [8], the concentrations of Ti, Nb and Zr may not correctly reflect the geodynamic setting of these rocks if their mantle sources were formed long before melt generation and emplacement.

This enriched mantle source of the Aldan shield could have a complex history that includes a stage of metasomatic enrichment that is related to the tectonic history of the region. Geochemical signatures similar to Chompolo rocks are characteristic for the Mesozoic potassic alkaline rocks of the Aldan shield [10,11,148]. As a result of the magmatic activity in the interval of J_1 – K_1 , several massifs of complex composition were formed (the Ryabinoviy, Yakokut, Tommot, Zametniy, Orto-Salaa, and Robkiy), as well as dyke swarms and diatremes (explosion pipes) in the north-central part of the Aldan shield (see large square, Figure 1) [10,12]. The close isotopic signatures of the enriched ancient mantle source are reflected in the rocks of Neoproterozoic lamprophyres of the Khani massif [149], as well as in the 1880 Ma Seligdar carbonatites (Figure 1) [122]. The model age calculated relative to the DM for the Ogonek pipe (2.35 Ga) is an estimate of the time when the depleted mantle of the Aldan shield underwent enrichment by LREE. This age is consistent with the model Nd and Hf ages calculated for alkaline rocks of the Central Aldan province, which are in the range of 1.5–3 Ga, with average values of about 2.0–2.1 Ga, and fall in the same line of Nd evolution as the Seligdar and Khani massifs [10,11,122]. These authors go on to suggest that a large amount of the enriched mantle source beneath the Aldan shield has undergone several melting episodes during post-Archean history, producing the series of rocks of the Aldrean alkaline province. The resulting model ages correspond to a long amalgamation period of the Siberian Craton and, in particular, the Aldan shield (2.5–2.6 and 2.1–1.9 Ga) [30,31]. The amalgamation of the terranes into the general structure of the Siberian Craton was inevitably accompanied by multiple subduction, collision and accretion events. In particular, the Central Aldan, Daldin and Tyung terranes formed a single amalgamated block accompanied by the Billyakh–Fedorov island arc and subducting oceanic crust under the newly formed microcontinent in the period 2500–2000 Ma [32,33]. Finally, during the Mesozoic tectono-magmatic activity of the central Aldan shield area, the ancient enriched mantle reservoir was melted, giving rise to diverse alkaline magmatism, including the lamprophyres of the Chompolo field.

6. Conclusions

Chompolo rocks are not kimberlites or lamproites but rather bear signatures of low-Ti lamprophyres on the basis of petrographic, mineralogical, and chemical criteria. ^{40}Ar – ^{39}Ar ages show that the Chompolo rocks were emplaced in the Late Jurassic or Early Cretaceous Periods.

Unlike the majority of “Aldan lamproites”, the Chompolo rocks contain xenocrysts of the minerals of their mantle origin, including mantle-derived pyroxenes. The lithospheric mantle in the area corresponds to the lithosphere of Precambrian cratons consisting of harzburgite–dunite, garnet and spinel lherzolite, and eclogite.

A two-stage model for the formation of Chomplo lamprophyres was suggested: (1) the formation of an isolated ancient enriched mantle source, and (2) the magma generation and emplacement stage. These stages are distant from each other in geological time. The unique trace element and isotopic characteristics of the ancient enriched source in the SCLM region, chemically isolated from the underlying convecting mantle, was formed as a result of the interaction with fluids and melts ascending from subducting slabs, approximately 2.4 billion years ago. This enriched source was formed during major episodes that amalgamated the Aldan superterrane in the Paleoproterozoic–Archean periods. During Mesozoic tectono-magmatic activity, this mantle source underwent partial melting. As a result, the rocks of the Aldan alkaline province, including the Chompolo field, were produced.

As the source of Chompolo lamprophyres spent a significant amount of time isolated from the asthenosphere, the lithospheric mantle in the area may have extended to a greater depth than was estimated by mantle xenocrysts, very probably into the diamond stability field. This leaves open the possibility to discover deeply derived, potentially diamond-bearing rocks in the Central Aldan area.

Supplementary Materials: The following are available online at <http://www.mdpi.com/2075-163X/10/10/886/s1>. Figure S1: Photomicrographs of mineral inclusions in the zonal diopside crystal from the Aldanskaya dyke (a–c—shown with increasing degree of magnification). Figure S2: The inverse isochron of $^{40}\text{Ar}/^{39}\text{Ar}$ study of 13Al507 (a) and 13Al613 (b) samples. Figure S3: Raman spectra of non-oriented richterite samples: a—K-F richterite (RRUFF ID: 835 R060034); b—K-richterite (sample XIII-83/5, Geological museum of IGM SB RAS); c—K-richterite from the Aldanskaya dyke. Figure S4: Cr-spinels from Chompolo field alkaline rocks in Al_2O_3 vs. Cr_2O_3 , TiO_2 vs. Cr_2O_3 , and $100 \times \text{Cr}/(\text{Cr} + \text{Al})$ vs. $100 \times \text{Fe}^{2+}/(\text{Fe}^{2+} + \text{Mg})$ plots. The left row shows data for the Sputnik and Ogonek pipes, and the right row shows the data for the Aldanskaya dike and the Perevalnaya and Gornaya pipes. Table S1: Results of $^{40}\text{Ar}/^{39}\text{Ar}$ study with stepwise heating of K-richterites from Chompolo rocks. Table S2: Representative compositions of the Cpx I and Cpx II clinopyroxene varieties in the Chompolo rocks. Table S3: Representative compositions of micas from the Sputnik pipe and the Aldanskaya dyke. Table S4: Mineral chemistry of amphiboles from the Aldanskaya dyke. Table S5: Representative compositions of pyrope xenocrysts from the Aldanskaya dyke, Ogonek, Gornaya, and Sputnik pipes. Table S6: Representative compositions of Cr-spinel xenocrysts from the Aldanskaya dyke, Ogonek, Sputnik, Gornaya, and Perevalnaya pipes. Table S7: Representative compositions of Cr-spinel xenocrysts from the Aldanskaya dyke (1–20); Ogonek (21–40); Sputnik (41, 60); Gornaya (61–80) and Perevalnaya (81–100) pipes. Table S8: Mineral chemistry of Ilmenites from the Chompolo lamprophyres. Table S9: Whole-rock major-oxide and trace-element compositions. Table S10: Sr-Nd isotopic ratios of Ogonek pipe rocks.

Author Contributions: Conceptualization and methodology, E.I.N., I.S.S.; resources, E.I.N., K.V.L., N.S.T., I.S.S., M.V.C.; formal analysis, E.I.N., A.M.A.; writing—original draft preparation, E.I.N., A.M.N.; writing—review and editing, E.I.N. and A.M.A.; supervision, A.M.A.; project administration, E.I.N., I.S.S.; funding acquisition, I.S.S., N.S.T., A.M.N. All authors have read and agreed to the published version of the manuscript.

Funding: Mineralogical, geochemical and isotopic studies were supported by the Russian Science Foundation (18-77-10062). The geochronological study was supported by the Russian Science Foundation (19-17-00019). Field trips for sample collection was funded by the state assignment of IGM SB RAS.

Acknowledgments: The authors thank the two anonymous reviewers for their insightful comments.

Conflicts of Interest: The authors declare no conflict of interest.

References

- Smith, M.; Moore, K.; Kavecsánszki, D.; Finch, A.A.; Kynicky, J.; Wall, F. From mantle to critical zone: A review of large and giant sized deposits of the rare earth elements. *Geosci. Front.* **2016**, *7*, 315–334. [CrossRef]
- Goodenough, K.M.; Wall, F.; Merriman, D. The rare earth elements: Demand, global resources, and challenges for resourcing future generations. *Nat. Resour. Res.* **2018**, *27*, 201–216. [CrossRef]
- Atkinson, W.; Smith, C.; Boxer, G. The discovery and geology of the Argyle diamond deposits, Kimberley, Western Australia. In Proceedings of the Darwin Conference, Australasian Institute of Mining and Metallurgy, Darwin City, Australia, 5–9 August 1984; pp. 141–149.
- Jaques, A.; Lewis, J.; Smith, C.; Gregory, G.; Ferguson, J.; Chappell, B.; McCulloch, M. The diamond-bearing ultrapotassic (lamproitic) rocks of the West Kimberley region, Western Australia. In *Developments in Petrology*; Elsevier: Amsterdam, The Netherlands, 1984; Volume 11, pp. 225–254.

5. Jaques, A.; Lewis, J.; Smith, C. The Kimberlites and Lamproites of Western Australia. *Geol. Surv. West. Aust. Bull.* **1986**, *132*, 268.
6. Kaminsky, F.V. Non-kimberlitic diamondiferous igneous rocks: 25 years on. *J. Geol. Soc. India* **2007**, *69*, 557.
7. Wyman, D.; Hollings, P.; Conceição, R. Geochemistry and radiogenic isotope characteristics of xenoliths in Archean diamondiferous lamprophyres: Implications for the Superior Province cratonic keel. *Lithos* **2015**, *233*, 111–130. [[CrossRef](#)]
8. Nelson, D.R. Isotopic characteristics of potassic rocks: Evidence for the involvement of subducted sediments in magma genesis. *Lithos* **1992**, *28*, 403–420. [[CrossRef](#)]
9. Vollmer, R. On the origin of the Italian potassic magmas: 1. A discussion contribution. *Chem. Geol.* **1989**, *74*, 229–239. [[CrossRef](#)]
10. Bogatkov, O.A.; Kononova, V.A.; Pervov, V.A.; Zhuravlev, D.Z. Petrogenesis of Mesozoic potassic magmatism of the Central Aldan: A Sr-Nd isotopic and geodynamic model. *Int. Geol. Rev.* **1994**, *36*, 629–644. [[CrossRef](#)]
11. Davies, G.; Stolz, A.; Mahotkin, I.; Nowell, G.; Pearson, D. Trace element and Sr–Pb–Nd–Hf isotope evidence for ancient, fluid-dominated enrichment of the source of Aldan Shield lamproites. *J. Petrol.* **2006**, *47*, 1119–1146. [[CrossRef](#)]
12. Maksimov, E.; Ugryumov, A. Mesozoic magmatic formations of the Aldan Shield. *Sov. Geol.* **1971**, *7*, 107–119.
13. Mues-Schumacher, U.; Keller, J.; Kononova, V.; Suddaby, P. Mineral chemistry and geochronology of the potassic alkaline ultramafic Inagli complex, Aldan Shield, eastern Siberia. *Mineral. Mag.* **1996**, *60*, 711–730. [[CrossRef](#)]
14. Bogatkov, O.; Ryabchikov, I.; Kononova, V.; Makhotkin, I.; Novgorodova, M.; Solovova, I.; Galuskin, E.; Ganeev, I.; Giris, A.; Eremeev, N.; et al. Lamproites. *Priroda. Moscow.* **1991**, *1991*, 302.
15. Kononova, V.; Bogatkov, O.; Kondrashov, I. Kimberlites and lamproites: Criteria for similarity and differences. *Petrology* **2011**, *19*, 34–54. [[CrossRef](#)]
16. Panina, L.; Vladyskin, N. Lamproitic rocks of the Murun Massif and their genesis. *Russ. Geol. Geophys.* **1994**, *35*, 100–113.
17. Vavilov, M.; Bazarova, Y.; Podgornyykh, N.; Krivoputskaya, L.; Kuznetsova, I. Characteristics and formation conditions of potassic alkaline rocks of the Loman Massif. *Russ. Geol. Geophys.* **1986**, *27*, 40–46.
18. Vladyskin, N. First find of lamproites in the USSR. *Proc. Dokl. Akad. Nauk SSSR* **1985**, *280*, 718–722.
19. Shilina, G.; Zeitlin, S. About the first finding of the kimberlites on Aldan shield. *Sov. Geol.* **1959**, *10*, 132–136.
20. Ashchepkov, I.; Vladyskin, N.; Ntaflos, T.; Kostrovitsky, S.; Prokopiev, S.; Downes, H.; Smelov, A.; Agashev, A.; Logvinova, A.; Kuligin, S.; et al. Layering of the lithospheric mantle beneath the Siberian Craton: Modeling using thermobarometry of mantle xenolith and xenocrysts. *Tectonophysics* **2014**, *634*, 55–75. [[CrossRef](#)]
21. Ashchepkov, I.; Pokhilenko, N.; Vladyskin, N.; Logvinova, A.; Afanas'ev, V.; Pokhilenko, L.N.; Kuligin, S.S.; Malygina, E.V.; Alymova, N.A.; Kostrovitsky, S.I.; et al. Structure and evolution of the lithospheric mantle beneath Siberian craton, thermobarometric study. *Tectonophysics* **2010**, *485*, 17–41. [[CrossRef](#)]
22. Ashchepkov, I.; Gerasimov, P.; Khmel'nikova, O.; Anoshin, G.; Vladyskin, N.; Saprykin, A. Temperature gradient and structure of the lithospheric block beneath the southeastern margin of the Siberian craton: Disintegrated xenolith evidence from kimberlitic pipes of the Aldan shield. In *Doklady Earth Sciences; Pleiades Publishing, Ltd.: New York, NY, USA*, 2001; Volume 378, pp. 495–499.
23. Kostrovitsky, S.; Garanin, V. High chromium titanates in pyropes dikes Aldan (Yakutia). *Zap. RMO* **1992**, *121*, 67–72.
24. Utrobin, D. On the Question of the Dismemberment of the Jurassic-Cretaceous Deposits of South Yakutia. In *Stratigraphy of the Precambrian and Phanerozoic of Transbaikalia and the south of the Far East*; Earth Sciences: Khabarovsk, Russia, 1990; pp. 223–225.
25. Kornilova, V. Petrography and mineralogy of the calc-alkaline lamprophyres and eruptive breccias at the basin of Chomppolo river. *Otechestvennaya Geol.* **1997**, *9*, 6–9.
26. Panina, L. Lamproite rocks of the Aldan and genetic criteria of lamproite melts. *Russ. Geol. Geophys.* **1993**, *34*, 82–94.
27. Rock, N. Nature and origin of calc-alkaline lamprophyres: Minettes, vogesites, kersantites and spessartites. *Earth Environ. Sci. Trans. R. Soc. Edinb.* **1984**, *74*, 193–227. [[CrossRef](#)]

28. Paquette, J.-L.; Ionov, D.A.; Agashev, A.; Gannoun, A.; Nikolenko, E. Age, provenance and Precambrian evolution of the Anabar shield from U-Pb and Lu-Hf isotope data on detrital zircons, and the history of the northern and central Siberian craton. *Precambrian Res.* **2017**, *301*, 134–144. [[CrossRef](#)]
29. Rosen, O. Siberian craton—a fragment of a Paleoproterozoic supercontinent. *Russ. J. Earth Sci.* **2002**, *4*, 103–119. [[CrossRef](#)]
30. Smelov, A.P.; Timofeev, V.F. The age of the North Asian Cratonic basement: An overview. *Gondwana Res.* **2007**, *12*, 279–288. [[CrossRef](#)]
31. Smelov, A.; Timofeev, V. The tectonics and metallogeny of the Precambrian of the Aldan-Stanovoy Shield. In *Mineral Deposit Research: Meeting the Global Challenge*; Springer: Berlin/Heidelberg, Germany, 2005; pp. 53–56.
32. Smelov, A.P.; Yan, H.; Timofeev, V.F.; Prokopiev, A.V.; Nokleberg, W.J. Archean through Mesoproterozoic metallogenesis and tectonics of northeast Asia. In *Metallogenesis and Tectonics of Northeast Asia*; US Geological Survey: Reston, VA, USA, 2010; Chapter 4.
33. Velikoslavinsky, S.; Kotov, A.; Sal'nikova, E.; Kovach, V.; Glebovitsky, V.; Zagornaya, N.Y.; Yakovleva, S.; Tolmacheva, E.; Anisimova, I.; Fedoseenko, A. Protoliths of the metamorphic rocks of the Fedorov Complex, Aldan Shield: Character, age, and geodynamic environments of origin. *Petrology* **2006**, *14*, 21–38. [[CrossRef](#)]
34. Mues, U. Geochemische und Radiometrische Untersuchungen an Lamproiten und Anderen Alkaligesteinen von Yakokut und Inagli, Aldan-Schild, Ostsibirien. Ph.D. Thesis, University of Freiburg, Freiburg, Germany, 1993.
35. Kononova, V.; Bogatkov, O.; Pervov, V.; Ereemeev, N.; Suddaby, P. Geochemistry and origin of the potassic magmatic rocks of the Central Aldan. *Geokhimiya* **1994**, *7*, 937–955.
36. Sorokin, A.A.; Zaika, V.A.; Kovach, V.P.; Kotov, A.B.; Xu, W.; Yang, H. Timing of closure of the eastern Mongol–Okhotsk Ocean: Constraints from U–Pb and Hf isotopic data of detrital zircons from metasediments along the Dzhangdy Transect. *Gondwana Res.* **2020**, *81*, 58–78. [[CrossRef](#)]
37. Vladimirov, N.; Dauv, Y.; Zubarev, B. *Geology and Genesis of Diamond Deposits*; TsNIGRI: Moscow, Russia, 1989.
38. Mudrik, S.; Anashin, M.; Pet'ko, V. *Report on the Results of Prospecting for Diamonds Held Alekseevskoy GPP on Ust-Tokkiskoy and Chompolinskoy Areas in 1986–1988 Years (unpublished)*; Yakutskgeology: Alekseevsk, Russia, 1988; p. 475.
39. Zaitsev, A.; Smelov, A. *Isotope Geochronology of Kimberlite Rocks in the Yakutian Province*; Ofset: Yakutsk, Russia, 2010; p. 108.
40. Lavrent'ev, Y.G.; Korolyuk, V.; Usova, L.; Nigmatulina, E. Electron probe microanalysis of rock-forming minerals with a JXA-8100 electron probe microanalyzer. *Russ. Geol. Geophys.* **2015**, *56*, 1428–1436. [[CrossRef](#)]
41. Nikolaeva, I.; Paleskii, S.; Koz'menko, O.; Anoshin, G. Analysis of geologic reference materials for REE and HFSE by inductively coupled plasma-mass spectrometry (ICP-MS). *Geochem. Int.* **2008**, *46*, 1016–1022. [[CrossRef](#)]
42. Travin, A.; Yudin, D.; Vladimirov, A.; Khromykh, S.; Volkova, N.; Mekhonoshin, A.; Kolotilina, T.B. Thermochronology of the Chernorud granulite zone, Ol'khon Region, Western Baikal area. *Geochem. Int.* **2009**, *47*, 1107–1124. [[CrossRef](#)]
43. Baksi, A.K.; Archibald, D.; Farrar, E. Intercalibration of $^{40}\text{Ar}/^{39}\text{Ar}$ dating standards. *Chem. Geol.* **1996**, *129*, 307–324. [[CrossRef](#)]
44. Lafuente, B.; Downs, R.; Yang, H.; Stone, N. The power of databases: The RRUFF project. In *Highlights in Mineralogical Crystallography*; Armbruster, T., Danisi, R.M., Eds.; De Gruyter: Berlin, Germany, 2015.
45. Pin, C.; Joannon, S.; Bosq, C.; Le Fevre, B.; Gauthier, P.-J. Precise determination of Rb, Sr, Ba, and Pb in geological materials by isotope dilution and ICP-quadrupole mass spectrometry following selective separation of the analytes. *J. Anal. Atom. Spectrom.* **2003**, *18*, 135–141. [[CrossRef](#)]
46. Bouvier, A.; Vervoort, J.D.; Patchett, P.J. The Lu–Hf and Sm–Nd isotopic composition of CHUR: Constraints from unequilibrated chondrites and implications for the bulk composition of terrestrial planets. *Earth Planet. Sci. Lett.* **2008**, *273*, 48–57. [[CrossRef](#)]
47. Goldstein, S.J.; Jacobsen, S.B. Nd and Sr isotopic systematics of river water suspended material: Implications for crustal evolution. *Earth Planet. Sci. Lett.* **1988**, *87*, 249–265. [[CrossRef](#)]
48. Whitney, D.L.; Evans, B.W. Abbreviations for names of rock-forming minerals. *Am. Mineral.* **2010**, *95*, 185–187. [[CrossRef](#)]
49. Khar'kiv, A.; Vishnevsky, A. Pyrope Megacrysts with the Features of Partial Melting from Yakutian Kimberlites. *Mineral. Zhur.* **1989**, *11*, 28–36.

50. Harrison, T.M. Diffusion of ^{40}Ar in hornblende. *Contrib. Mineral. Petrol.* **1982**, *78*, 324–331. [[CrossRef](#)]
51. Whitehead, J.; Reynolds, P.H.; Spray, J.G. $^{40}\text{Ar}/^{39}\text{Ar}$ age constraints on Taconian and Acadian events in the Quebec Appalachians. *Geology* **1996**, *24*, 359–362. [[CrossRef](#)]
52. Rock, N. The International Mineralogical Association (IMA/CNMMN) pyroxene nomenclature scheme: Computerization and its consequences. *Mineral. Petrol.* **1990**, *43*, 99–119. [[CrossRef](#)]
53. Mitchell, R.H. Kimberlites and orangeites. In *Kimberlites, Orangeites, and Related Rocks*; Springer: Berlin/Heidelberg, Germany, 1995; pp. 1–90.
54. Mitchell, R.H.; Bergman, S.C. *Petrology of Lamproites*; Springer Science & Business Media: Berlin, Germany, 1991.
55. Tappe, S.; Foley, S.F.; Jenner, G.A.; Heaman, L.M.; Kjarsgaard, B.A.; Romer, R.L.; Stracke, A.; Joyce, N.; Hoefs, J. Genesis of ultramafic lamprophyres and carbonatites at Aillik Bay, Labrador: A consequence of incipient lithospheric thinning beneath the North Atlantic craton. *J. Petrol.* **2006**, *47*, 1261–1315. [[CrossRef](#)]
56. Grütter, H.S.; Gurney, J.J.; Menzies, A.H.; Winter, F. An updated classification scheme for mantle-derived garnet, for use by diamond explorers. *Lithos* **2004**, *77*, 841–857. [[CrossRef](#)]
57. Sobolev, N.; Lavrent'Ev, Y.G.; Pokhilenko, N.; Usova, L. Chrome-rich garnets from the kimberlites of Yakutia and their parageneses. *Contrib. Mineral. Petrol.* **1973**, *40*, 39–52. [[CrossRef](#)]
58. Fitzpayne, A.; Giuliani, A.; Hergt, J.; Phillips, D.; Janney, P. New geochemical constraints on the origins of MARID and PIC rocks: Implications for mantle metasomatism and mantle-derived potassic magmatism. *Lithos* **2018**, *318*, 478–493. [[CrossRef](#)]
59. Wyman, D.; Kerrich, R. Archean shoshonitic lamprophyres of the Abitibi Subprovince, Canada: Petrogenesis, age, and tectonic setting. *J. Petrol.* **1993**, *34*, 1067–1109. [[CrossRef](#)]
60. Pandey, A.; Rao, N.C.; Pandit, D.; Pankaj, P.; Pandey, R.; Sahoo, S.; Kumar, A. Subduction–Tectonics in the evolution of the eastern Dharwar craton, southern India: Insights from the post-collisional calc-alkaline lamprophyres at the western margin of the Cuddapah basin. *Precambrian Res.* **2017**, *298*, 235–251. [[CrossRef](#)]
61. Pandey, A.; Rao, N.C.; Chakrabarti, R.; Pankaj, P.; Pandit, D.; Pandey, R.; Sahoo, S. Post-collisional calc-alkaline lamprophyres from the Kadiri greenstone belt: Evidence for the Neoproterozoic convergence-related evolution of the Eastern Dharwar Craton and its schist belts. *Lithos* **2018**, *320*, 105–117. [[CrossRef](#)]
62. Lanjewar, S.; Randive, K. Lamprophyres from the Harohalli dyke swarm in the Halaguru and Mysore areas, Southern India: Implications for backarc basin magmatism. *J. Asian Earth Sci.* **2018**, *157*, 329–347. [[CrossRef](#)]
63. Choi, E.; Fiorentini, M.L.; Giuliani, A.; Foley, S.F.; Maas, R.; Taylor, W.R. Subduction-related petrogenesis of Late Archean calc-alkaline lamprophyres in the Yilgarn Craton (Western Australia). *Precambrian Res.* **2020**, *338*, 105550. [[CrossRef](#)]
64. Carmichael, I.S. The mineralogy and petrology of the volcanic rocks from the Leucite Hills, Wyoming. *Contrib. Mineral. Petrol.* **1967**, *15*, 24–66. [[CrossRef](#)]
65. Hwang, P.; Taylor, W.; Rocky, N.; Ramsay, R. Mineralogy, geochemistry and petrogenesis of the Metters Bore No. 1 lamproite pipe, Calwynyardah Field, West Kimberley Province, Western Australia. *Miner. Petrol.* **1994**, *51*, 195–226. [[CrossRef](#)]
66. Reddy, T.A.K. Petrography and geochemistry of the Krishna lamproite field, Andhra Pradesh. *J. Geol. Soc. India* **2003**, *61*, 131–14.
67. Kravchenko, S. Porphyric alkaline-ultrabasic potassic rocks of the central Tomtor Massif (Arctic Siberia): Carbonatized lamproites. *Russ. Geol. Geophys.* **2003**, *44*, 906–918.
68. Rao, N.C.; Gibson, S.; Pyle, D.; Dickin, A. Petrogenesis of Proterozoic lamproites and kimberlites from the Cuddapah Basin and Dharwar craton, southern India. *J. Petrol.* **2004**, *45*, 907–948. [[CrossRef](#)]
69. Rao, N.C.; Kamde, G.; Kale, H.; Dongre, A. Petrogenesis of the Mesoproterozoic lamproites from the Krishna valley, eastern Dharwar craton, southern India. *Precambrian Res.* **2010**, *177*, 103–130. [[CrossRef](#)]
70. Rukhlov, A.S.; Blinova, A.I.; Pawlowicz, J.G. Geochemistry, mineralogy and petrology of the Eocene potassic magmatism from the Milk River area, southern Alberta, and Sweet Grass Hills, northern Montana. *Chem. Geol.* **2013**, *353*, 280–302. [[CrossRef](#)]
71. Shaikh, A.M.; Patel, S.; Ravi, S.; Behera, D.; Pruseth, K. Mineralogy of the TK1 and TK4 ‘kimberlites’ in the Timmasamudram cluster, Wajrakarur Kimberlite Field, India: Implications for lamproite magmatism in a field of kimberlites and ultramafic lamprophyres. *Chem. Geol.* **2017**, *455*, 208–230. [[CrossRef](#)]

72. Talukdar, D.; Pandey, A.; Rao, N.C.; Kumar, A.; Pandit, D.; Belyatsky, B.; Lehmann, B. Petrology and geochemistry of the Mesoproterozoic Vattikod lamproites, Eastern Dharwar Craton, southern India: Evidence for multiple enrichment of sub-continental lithospheric mantle and links with amalgamation and break-up of the Columbia supercontinent. *Contrib. Mineral. Petrol.* **2018**, *173*, 67. [\[CrossRef\]](#)
73. Prelević, D.; Akal, C.; Foley, S.; Romer, R.; Stracke, A.; Van Den Bogaard, P. Ultrapotassic mafic rocks as geochemical proxies for post-collisional dynamics of orogenic lithospheric mantle: The case of southwestern Anatolia, Turkey. *J. Petrol.* **2012**, *53*, 1019–1055. [\[CrossRef\]](#)
74. Çoban, H.; Flower, M.F. Mineral phase compositions in silica-undersaturated ‘leucite’ lamproites from the Bucak area, Isparta, SW Turkey. *Lithos* **2006**, *89*, 275–299. [\[CrossRef\]](#)
75. Akal, C. K-richterite–olivine–phlogopite–diopside–sanidine lamproites from the Afyon volcanic province, Turkey. *Geol. Mag.* **2008**, *145*, 570–585. [\[CrossRef\]](#)
76. Tappe, S.; Foley, S.F.; Stracke, A.; Romer, R.L.; Kjarsgaard, B.A.; Heaman, L.M.; Joyce, N. Craton reactivation on the Labrador Sea margins: 40Ar/39Ar age and Sr–Nd–Hf–Pb isotope constraints from alkaline and carbonatite intrusives. *Earth Planet. Sci. Lett.* **2007**, *256*, 433–454. [\[CrossRef\]](#)
77. Nikolenko, E.; Afanas’ev, V.; Pokhilenko, N. Garnets of crustal parageneses in alluvial deposits of the eastern Siberian Platform: Genesis and search significance. *Russ. Geol. Geophys.* **2008**, *49*, 655–666. [\[CrossRef\]](#)
78. Tychkov, N.; Pokhilenko, N.; Kuligin, S.; Malygina, E. Composition and origin of peculiar pyropes from lherzolites: Evidence for the evolution of the lithospheric mantle of the Siberian Platform. *Russ. Geol. Geophys.* **2008**, *49*, 225–239. [\[CrossRef\]](#)
79. Sobolev, N.; Lavrent’ev, Y.; Pospelova, L.; Sobolev, E. Chrome pyropes from the diamonds of Yakutia. *Dokl. Akad. Nauk SSSR* **1969**, *189*, 162–165.
80. Schulze, D.J. A classification scheme for mantle-derived garnets in kimberlite: A tool for investigating the mantle and exploring for diamonds. *Lithos* **2003**, *71*, 195–213. [\[CrossRef\]](#)
81. Sobolev, N. On mineralogical criteria of a diamond potential of kimberlites. *Geol. I Geofiz.* **1971**, *12*, 70–78.
82. Kampata, M.; Moreau, J.; Hertogen, J.; Demaiffe, D.; Condliffe, E.; Mvuemba, N. Megacrysts and ultramafic xenoliths from Kundelungu kimberlites (Shaba, Zaire). *Mineral. Mag.* **1995**, *59*, 661–676. [\[CrossRef\]](#)
83. Robles-Cruz, S.E.; Watangua, M.; Isidoro, L.; Melgarejo, J.C.; Galí, S.; Olimpio, A. Contrasting compositions and textures of ilmenite in the Catoca kimberlite, Angola, and implications in exploration for diamond. *Lithos* **2009**, *112*, 966–975. [\[CrossRef\]](#)
84. Nikolenko, E.; Afanas’ev, V.; Pokhilenko, N. Peculiarities of the composition of zoned picroilmenites from the Massadou field (Giunea) and Dachnaya pipe (Yakutia) kimberlites. *Dokl. Earth. Sci.* **2010**, *434*, 1386. [\[CrossRef\]](#)
85. Foley, S.; Venturelli, G.; Green, D.; Toscani, L. The ultrapotassic rocks: Characteristics, classification, and constraints for petrogenetic models. *Earth-Sci. Rev.* **1987**, *24*, 81–134. [\[CrossRef\]](#)
86. Irvine, T.; Baragar, W. A guide to the chemical classification of the common volcanic rocks. *Can. J. Earth Sci.* **1971**, *8*, 523–548. [\[CrossRef\]](#)
87. Kostrovitsky, S.; Morikiyo, T.; Serov, I.; Yakovlev, D.; Amirzhanov, A. Isotope-geochemical systematics of kimberlites and related rocks from the Siberian Platform. *Russ. Geol. Geophys.* **2007**, *48*, 272–290. [\[CrossRef\]](#)
88. Mirnejad, H.; Bell, K. Origin and source evolution of the Leucite Hills lamproites: Evidence from Sr–Nd–Pb–O isotopic compositions. *J. Petrol.* **2006**, *47*, 2463–2489. [\[CrossRef\]](#)
89. Chen, Y.; Yao, S.; Pan, Y. Geochemistry of lamprophyres at the Daping gold deposit, Yunnan Province, China: Constraints on the timing of gold mineralization and evidence for mantle convection in the eastern Tibetan Plateau. *J. Asian Earth Sci.* **2014**, *93*, 129–145. [\[CrossRef\]](#)
90. Chen, B.; Zhai, M. Geochemistry of late Mesozoic lamprophyre dykes from the Taihang Mountains, north China, and implications for the sub-continental lithospheric mantle. *Geol. Mag.* **2003**, *140*, 87–93. [\[CrossRef\]](#)
91. Wyman, D.; Ayer, J.; Conceição, R.; Sage, R. Mantle processes in an Archean orogen: Evidence from 2.67 Ga diamond-bearing lamprophyres and xenoliths. *Lithos* **2006**, *89*, 300–328. [\[CrossRef\]](#)
92. Wyman, D.; Kerrich, R. Archean lamprophyre dikes of the Superior Province, Canada: Distribution, petrology, and geochemical characteristics. *J. Geophys. Res.-Sol. Ea.* **1989**, *94*, 4667–4696. [\[CrossRef\]](#)
93. Leat, P.; Thompson, R.; Morrison, M.; Hendry, G.; Dickin, A. Silicic magmas derived by fractional crystallization from Miocene minette, Elkhead Mountains, Colorado. *Mineral. Mag.* **1988**, *52*, 577–585. [\[CrossRef\]](#)

94. Sun, S.-S.; McDonough, W.F. Chemical and isotopic systematics of oceanic basalts: Implications for mantle composition and processes. *J. Geol. Soc. Lond.* **1989**, *42*, 313–345. [[CrossRef](#)]
95. McDonough, W.F.; Sun, S.-S. The composition of the Earth. *Chem. Geol.* **1995**, *120*, 223–253. [[CrossRef](#)]
96. Kempton, P.; Fitton, J.; Hawkesworth, C.; Ormerod, D. Isotopic and trace element constraints on the composition and evolution of the lithosphere beneath the southwestern United States. *J. Geophys. Res.-Sol. Earth* **1991**, *96*, 13713–13735. [[CrossRef](#)]
97. Wannamaker, P.E.; Hulen, J.B.; Heizler, M.T. Early Miocene lamproite from the Colorado Plateau tectonic province, southeastern Utah, USA. *J. Volcanol. Geotherm. Res.* **2000**, *96*, 175–190. [[CrossRef](#)]
98. Schleicher, H.; Lippolt, H.J.; Raczek, I. Rb-Sr systematics of Permian volcanites in the Schwarzwald (SW-Germany). *Contrib. Mineral. Petrol.* **1983**, *84*, 281–291. [[CrossRef](#)]
99. Wright, J. The phonolite-trachyte spectrum. *Lithos* **1971**, *4*, 1–5. [[CrossRef](#)]
100. Ehrenberg, S.N. Garnetiferous ultramafic inclusions in minette from the Navajo volcanic field. *Mantle Sample Incl. Kimberl. Other Volcan.* **1979**, *16*, 330–344. [[CrossRef](#)]
101. Panina, L. Low-titanium Aldan lamproites (Siberia): Melt inclusions in minerals. *Russ. Geol. Geophys.* **1997**, *38*, 118–127.
102. Vladyskin, N. Geochemistry and genesis of lamproites of the Aldan Shield. In Proceedings of the International Kimberlite Conference: Extended Abstracts, Novosibirsk, Russia, 19 September 1995; Volume 6, pp. 660–662.
103. Nikolenko, E.I.; Sharygin, I.S.; Alifirova, T.A.; Korsakov, A.V.; Zelenovskiy, P.S.; Shur, V.Y. Graphite-bearing mineral assemblages in the mantle beneath Central Aldan superterrane of North Asian craton: Combined confocal micro-Raman and electron microprobe characterization. *J. Raman Spectrosc.* **2017**, *48*, 1597–1605. [[CrossRef](#)]
104. Ashchepkov, I.; Vladyskin, N.; Saprykin, A.; Khmelnikova, O.; Anoshin, G. Composition and thermal structure of the mantle in peripheral parts of Siberian craton. *Rev. Bras. Geo.* **2001**, *31*, 527–536. [[CrossRef](#)]
105. Le Maitre, R.; Streckeisen, A.; Zanettin, B.; Le Bas, M.; Bonin, B.; Bateman, P. *Igneous Rocks: A Classification and Glossary of Terms: Recommendations of the International Union of Geological Sciences Subcommittee on the Systematics of Igneous Rocks*; Cambridge University Press: Cambridge, UK, 2005.
106. Vasilenko, V.; Zinchuk, N.; Kuznetsova, L. *Petrochemical Models for Diamond Deposits in Yakutia*; Nauka Novosibirsk: Moscow, Russia, 1997. (In Russian)
107. Mitchell, R.H.; Giuliani, A.; O'Brien, H. What is a kimberlite? Petrology and mineralogy of hypabyssal kimberlites. *Elem. Int. Mag. Mineral. Geochem. Petrol.* **2019**, *15*, 381–386. [[CrossRef](#)]
108. Cox, K.G. *The Interpretation of Igneous Rocks*; Springer Science & Business Media: Berlin, Germany, 2013.
109. Woolley, A.R.; Bergman, S.C.; Edgar, A.D.; Le Bas, M.J.; Mitchell, R.H.; Rock, N.M.; Scott Smith, B.H. Classification of lamprophyres, lamproites, kimberlites, and the kalsilitic, melilitic, and leucitic rocks. *Can. Mineral.* **1996**, *34*, 175–186.
110. Rock, N.; Bowes, D.; Wright, A. *Lamprophyres*; Blackie: Glasgow, UK, 1991.
111. Mitchell, R.H. *Kimberlites: Mineralogy, Geochemistry, and Petrology*; Springer Science & Business Media: Berlin, Germany, 2013.
112. Nemec, D. Origin of syenite porphyries in the Central Bohemian Pluton by magma mixing. *Neues Jahrb. Mineral. Abh.* **1988**, *159*, 59–71.
113. Zliao, D.; Smith, D.; Yang, J.; Deng, C.; Huang, Y. The Yinniugou lamproites in datong, Northern Shanxi province, China: First occurrence in the North China craton. In Proceedings of the Mid-Continent Diamonds: GAC-MAC Symposium Volume, Edmonton, Alberta, 17–18 May 1993; p. 139.
114. Sharygin, I.S.; Nikolenko, E.I.; Lobov, K.V. Carbonate inclusions in Cr-pyropes derived from the mantle beneath Central Aldan superterrane of Siberian craton. In Proceedings of the International Kimberlite Conference: Extended Abstracts, Gaborone, Botswana, 18–22 September 2017; Volume 11, pp. 1–3.
115. Exley, R.; Smith, J. The role of apatite in mantle enrichment processes and in the petrogenesis of some alkali basalt suites. *Geochim. Cosmochim. Acta* **1982**, *46*, 1375–1384. [[CrossRef](#)]
116. Smith, B.S.; Skinner, E. A new look at Prairie Creek, Arkansas. In *Developments in Petrology*; Elsevier: Amsterdam, The Netherlands, 1984; Volume 11, pp. 255–283.
117. Soltys, A.; Giuliani, A.; Phillips, D. Apatite compositions and groundmass mineralogy record divergent melt/fluid evolution trajectories in coherent kimberlites caused by differing emplacement mechanisms. *Contrib. Mineral. Petrol.* **2020**, *175*. [[CrossRef](#)]

118. Dalton, H.; Giuliani, A.; O'Brien, H.; Phillips, D.; Hergt, J.; Maas, R. Petrogenesis of a hybrid cluster of evolved kimberlites and ultramafic lamprophyres in the Kuusamo area, Finland. *J. Petrol.* **2019**, *60*, 2025–2050. [[CrossRef](#)]
119. Bergman, S.C. Lamproites and other potassium-rich igneous rocks: A review of their occurrence, mineralogy and geochemistry. *GSL SP* **1987**, *30*, 103–190. [[CrossRef](#)]
120. Rock, N.M. The nature and origin of lamprophyres: An overview. *J. Geol. Soc. Lond.* **1987**, *30*, 191–226. [[CrossRef](#)]
121. Vladyskin, N. Potassium alkaline lamproite-carbonatite complexes: Petrology, genesis, and ore reserves. *Russ. Geol. Geophys.* **2009**, *50*, 1119–1128. [[CrossRef](#)]
122. Doroshkevich, A.G.; Prokopyev, I.R.; Izokh, A.E.; Klemm, R.; Ponomarchuk, A.V.; Nikolaeva, I.V.; Vladyskin, N.V. Isotopic and trace element geochemistry of the Seligdar magnesiocarbonatites (South Yakutia, Russia): Insights regarding the mantle evolution beneath the Aldan-Stanovoy shield. *J. Asian Earth Sci.* **2018**, *154*, 354–368. [[CrossRef](#)]
123. Scambelluri, M.; Van Roermund, H.L.; Pettke, T. Mantle wedge peridotites: Fossil reservoirs of deep subduction zone processes: Inferences from high and ultrahigh-pressure rocks from Bardane (Western Norway) and Ulten (Italian Alps). *Lithos* **2010**, *120*, 186–201. [[CrossRef](#)]
124. Bebout, G.E. Metasomatism in subduction zones of subducted oceanic slabs, mantle wedges, and the slab-mantle interface. In *Metasomatism and the Chemical Transformation of Rock*; Springer: Berlin, Germany, 2013; pp. 289–349.
125. Plank, T. Constraints from thorium/lanthanum on sediment recycling at subduction zones and the evolution of the continents. *JPET* **2005**, *46*, 921–944. [[CrossRef](#)]
126. Pearce, J.A. Role of the sub-continental lithosphere in magma genesis at active continental margins. In *Continental Basalts and Mantle Xenoliths*; Shiva Publications: Nantwich, UK, 1983; pp. 230–249.
127. Rudnick, R.; Gao, S. Composition of the continental crust. *Crust* **2003**, *3*, 1–64. [[CrossRef](#)]
128. Pearce, J. Geochemical fingerprinting of oceanic basalts with applications to ophiolite classification and the search for Archean oceanic crust. *Lithos* **2008**, *14*–48. [[CrossRef](#)]
129. Turner, S.; Arnaud, N.; Liu, J.; Rogers, N.; Hawkesworth, C.; Harris, N.; Kelley, S.; Van Calsteren, P.; Deng, W. Post-collision, shoshonitic volcanism on the Tibetan Plateau: Implications for convective thinning of the lithosphere and the source of ocean island basalts. *J. Petrol.* **1996**, *37*, 45–71. [[CrossRef](#)]
130. Williams, H.M.; Turner, S.P.; Pearce, J.A.; Kelley, S.; Harris, N. Nature of the source regions for post-collisional, potassic magmatism in southern and northern Tibet from geochemical variations and inverse trace element modelling. *J. Petrol.* **2004**, *45*, 555–607. [[CrossRef](#)]
131. Plank, T. *The Chemical Composition of Subducting Sediments*; Elsevier: Amsterdam, The Netherlands, 2014.
132. Guo, Z.; Wilson, M. The Himalayan leucogranites: Constraints on the nature of their crustal source region and geodynamic setting. *Gondwana Res.* **2012**, *22*, 360–376. [[CrossRef](#)]
133. Kepezhinskas, P.; McDermott, F.; Defant, M.J.; Hochstaedter, A.; Drummond, M.S.; Hawkesworth, C.J.; Koloskov, A.; Maury, R.C.; Bellon, H. Trace element and Sr Nd Pb isotopic constraints on a three-component model of Kamchatka Arc petrogenesis. *Geochim. Cosmochim. Acta* **1997**, *61*, 577–600. [[CrossRef](#)]
134. Hofmann, A.W. Chemical differentiation of the Earth: The relationship between mantle, continental crust, and oceanic crust. *Earth Planet. Sci. Lett.* **1988**, *90*, 297–314. [[CrossRef](#)]
135. Bulatov, V.; Brey, G.; Gurnis, A.; Gerdes, A.; Höfer, H. Carbonated sediment–peridotite interaction and melting at 7.5–12 GPa. *Lithos* **2014**, *200*, 368–385. [[CrossRef](#)]
136. Stalder, R.; Foley, S.; Brey, G.; Horn, I. Mineral–aqueous fluid partitioning of trace elements at 900–1200 °C and 3.0–5.7 GPa: New experimental data for garnet, clinopyroxene, and rutile, and implications for mantle metasomatism. *Geochim. Cosmochim. Acta* **1998**, *62*, 1781–1801. [[CrossRef](#)]
137. Anders, E.; Grevesse, N. Abundances of the elements: Meteoritic and solar. *Geochim. Cosmochim. Acta* **1989**, *53*, 197–214. [[CrossRef](#)]
138. Gao, Y.; Hou, Z.; Kamber, B.S.; Wei, R.; Meng, X.; Zhao, R. Lamproitic rocks from a continental collision zone: Evidence for recycling of subducted Tethyan oceanic sediments in the mantle beneath southern Tibet. *J. Petrol.* **2007**, *48*, 729–752. [[CrossRef](#)]
139. Su, H.-M.; Jiang, S.-Y.; Zhang, D.-Y.; Wu, X.-K. Partial melting of subducted sediments produced early Mesozoic calc-alkaline lamprophyres from northern Guangxi Province, South China. *Sci. Rep.* **2017**. [[CrossRef](#)] [[PubMed](#)]

140. Feldstein, S.N.; Lange, R.A. Pliocene potassic magmas from the Kings River region, Sierra Nevada, California: Evidence for melting of a subduction-modified mantle. *J. Petrol.* **1999**, *40*, 1301–1320. [[CrossRef](#)]
141. Furman, T.; Graham, D. Erosion of lithospheric mantle beneath the East African Rift system: Geochemical evidence from the Kivu volcanic province. In *Developments in Geotectonics*; Elsevier: Amsterdam, The Netherlands, 1999; Volume 24, pp. 237–262.
142. Guo, Z.; Hertogen, J.; Liu, J.; Pasteels, P.; Boven, A.; Punzalan, L.; He, H.; Luo, X.; Zhang, W. Potassic magmatism in western Sichuan and Yunnan provinces, SE Tibet, China: Petrological and geochemical constraints on petrogenesis. *J. Petrol.* **2004**, *46*, 33–78. [[CrossRef](#)]
143. Konzett, J.; Wirth, R.; Hauzenberger, C.; Whitehouse, M. Two episodes of fluid migration in the Kaapvaal Craton lithospheric mantle associated with Cretaceous kimberlite activity: Evidence from a harzburgite containing a unique assemblage of metasomatic zirconium-phases. *Lithos* **2013**, *182*, 165–184. [[CrossRef](#)]
144. Rezvukhin, D.I.; Malkovets, V.G.; Sharygin, I.S.; Tretiakova, I.G.; Griffin, W.L.; O'Reilly, S.Y. Inclusions of crichtonite-group minerals in Cr-pyropes from the Internatsionalnaya kimberlite pipe, Siberian Craton: Crystal chemistry, parageneses and relationships to mantle metasomatism. *Lithos* **2018**, *308*, 181–195. [[CrossRef](#)]
145. Rezvukhin, D.; Nikolenko, E.; Sharygin, I.; Malkovets, V. Oxide mineral inclusions in Cr-pyropes from the Aldanskaya lamprophyre dyke, Yakutia. In *Proceedings of the Magmatism of the Earth and Related Strategic Metal Deposits*, Miass, Russia, 4–9 August 2017; pp. 205–208.
146. Alifirova, T.; Rezvukhin, D.; Nikolenko, E.; Pokhilenko, L.; Zelenovskiy, P.; Sharygin, I.; Korsakov, A.; Shur, V. Micro-Raman study of crichtonite group minerals enclosed into mantle garnet. *J. Raman Spectrosc.* **2020**, *51*, 1493–1512. [[CrossRef](#)]
147. Lustrino, M.; Agostini, S.; Chalal, Y.; Fedele, L.; Stagno, V.; Colombi, F.; Bouguerra, A. Exotic lamproites or normal ultrapotassic rocks? The Late Miocene volcanic rocks from Kef Hahouner, NE Algeria, in the frame of the circum-Mediterranean lamproites. *J. Volcanol. Geotherm. Res.* **2016**, *327*, 539–553. [[CrossRef](#)]
148. Mitchell, R.; Smith, C.; Vladyskin, N. Isotopic composition of strontium and neodymium in potassic rocks of the Little Murun complex, Aldan Shield, Siberia. *Lithos* **1994**, *32*, 243–248. [[CrossRef](#)]
149. Vladyskin, N.; Morikiyo, T.; Miyazaki, T. Sr and Nd isotopes geochemistry of alkaline and carbonatite complexes of Siberia and Mongolia and some geodynamic consequences. In *Proceedings of the 5th International Conference “Problems of Sources of Deep Magmatism and Plumes”*, Petropavlovsk-Kamchatskiy, Russia, 23 October 2005; pp. 19–37.



© 2020 by the authors. Licensee MDPI, Basel, Switzerland. This article is an open access article distributed under the terms and conditions of the Creative Commons Attribution (CC BY) license (<http://creativecommons.org/licenses/by/4.0/>).